5-1-2020

Wnt regulation: Exploring Axin-Disheveled interactions and defining mechanisms by which the SCF E3 ubiquitin ligase is recruited to the destruction complex

Kristina N. Schaefer

Mira I. Pronobis

Clara E. Williams

Shiping Zhang

Lauren Bauer

See next page for additional authors

Authors

Kristina N. Schaefer, Mira I. Pronobis, Clara E. Williams, Shiping Zhang, Lauren Bauer, Dennis Goldfarb, Feng Yan, M Ben Major, and Mark Peifer

Wnt regulation: exploring Axin-Disheveled interactions and defining mechanisms by which the SCF E3 ubiquitin ligase is recruited to the destruction complex

Kristina N. Schaefer[a], Mira I. Pronobis[a], Clara E. Williams[b], Shiping Zhang[b], Lauren Bauer[b], Dennis Goldfarb[c,d,e], Feng Yan[c], M. Ben Major[c,d,f,g], and Mark Peifer[a,b,c,*]

[a]Curriculum in Genetics and Molecular Biology, [b]Department of Biology, [c]Lineberger Comprehensive Cancer Center, and [f]Department of Cell Biology and Physiology, University of North Carolina at Chapel Hill, Chapel Hill, NC 27599; [d]Department of Cell Biology and Physiology, [e]Institute for Informatics, and [g]Department of Otolaryngology, Washington University School of Medicine, St. Louis, MO 63110

ABSTRACT **Wnt signaling plays key roles in embryonic development and adult stem cell homeostasis and is altered in human cancer. Signaling is turned on and off by regulating stability of the effector β-catenin (β-cat). The multiprotein destruction complex binds and phosphorylates β-cat and transfers it to the SCF-TrCP E3-ubiquitin ligase for ubiquitination and destruction. Wnt signals act though Dishevelled to turn down the destruction complex, stabilizing β-cat. Recent work clarified underlying mechanisms, but important questions remain. We explore β-cat transfer from the destruction complex to the E3 ligase, and test models suggesting Dishevelled and APC2 compete for association with Axin. We find that Slimb/TrCP is a dynamic component of the destruction complex biomolecular condensate, while other E3 proteins are not. Recruitment requires Axin and not APC, and Axin's RGS domain plays an important role. We find that elevating Dishevelled levels in *Drosophila* embryos has paradoxical effects, promoting the ability of limiting levels of Axin to turn off Wnt signaling. When we elevate Dishevelled levels, it forms its own cytoplasmic puncta, but these do not recruit Axin. Superresolution imaging in mammalian cells raises the possibility that this may result by promoting Dishevelled:Dishevelled interactions at the expense of Dishevelled: Axin interactions when Dishevelled levels are high.**

Monitoring Editor
Richard Fehon
University of Chicago

Received: Nov 18, 2019
Revised: Feb 12, 2020
Accepted: Feb 26, 2020

INTRODUCTION

During embryonic development, cells must choose fate based on their position within the unfolding body plan. One key is cell–cell signaling, by which cells communicate positional information to neighbors and ultimately direct downstream transcriptional programs. A small number of conserved signaling pathways play an inordinately important role in these events in all animals. These include the Hedgehog, Notch, Receptor Tyrosine kinase, BMP/TGFβ, and Wnt pathways, which influence development of most tissues and organs (Basson, 2012). These same signaling pathways regulate tissue stem cells during tissue homeostasis and play critical roles in

This article was published online ahead of print in MBoC in Press (http://www.molbiolcell.org/cgi/doi/10.1091/mbc.E19-11-0647) on March 4, 2020.

Author contributions: K.N.S, M.I.P. and M.P. conceived the study; K.N.S. led the experimental team; K.N.S. analyzed the effects of Dsh/Axin coexpression, with assistance from C.E.W. and analysis of Dsh localization by S.Z.; K.N.S., and M.I.P. analyzed the interactions of the destruction complex with E3 ligase proteins, with help from L.B.; M.I.P. carried out mass spectroscopy in collaboration with F.Y. and M.B.M.; and D.G. analyzed the resulting data. All other experiments were carried out by K.N.S. K.N.S., M.I.P., and M.P. wrote the manuscript with input from the other authors. CRediT Taxonomy is as follows: Conceptualization: K.N.S., M.I.P., and M.P.; investigation: K.N.S., M.I.P., C.E.W., L.B., F.Y., M.B.M., D.G., and M. P.; supervision: K.N.S. and M. P.; writing: original draft preparation, K.N.S., M.I.P., and M. P.; writing: review and editing, K.N.S., M.I.P., C.E.W., L.B., F.Y., M.B.M., D.G., and M. P.; funding acquisition: K.N.S., M.I.P., and M.P.

*Address correspondence to: Mark Peifer (peifer@unc.edu).

Abbreviations used: APC, adenomatous polyposis coli; Arm, Armadillo; β-cat, β-catenin; CK1, casein kinase 1; co-IP, coimmunoprecipitate; Cul1, Cullin1; DSHB, Developmental Studies Hybridoma Bank; En, engrailed; FRAP, fluorescence recovery after photobleaching; GSK3, glycogen synthase kinase 3; IP, immunoprecipitation; LFQ, label-free quantification; MS, mass spectrometry; NGS, normal goat serum; PBS, phosphate-buffered saline; RBX, Ring box; SCF, Skp-Cullin-F-box; SIM, structured illumination microscopy.

most solid tumors. Due to their powerful effects on cell fate and behavior, evolution has shaped dedicated machinery that keeps each signaling pathway definitively off in the absence of ligand.

In the Wnt pathway, signaling is turned on and off by regulating stability of the key effector β-catenin (βcat; reviewed in Nusse and Clevers, 2017). In the absence of Wnt ligands, newly synthesized βcat is rapidly captured by the multiprotein destruction complex (Figure 1A). Within this complex, the protein Axin acts as a scaffold, recruiting multiple partners. Axin and adenomatous polyposis coli (APC) bind βcat and present it to the kinases casein kinase 1 (CK1) and glycogen synthase kinase 3 (GSK3) for sequential phosphorylation of a series of N-terminal serine and threonine residues on βcat.

It has become increasingly clear that the destruction complex is not a simple four-protein entity. Instead, Axin directs assembly of destruction complex proteins into what the field originally described as "puncta." We now recognize these as examples of supermolecular, nonmembrane bound cellular compartments (reviewed in Gammons and Bienz, 2017; Schaefer and Peifer, 2019), referred to as biomolecular condensates (Banani *et al.*, 2017). Condensate formation is driven by Axin polymerization via its DIX domain, by APC function, and by other multivalent interactions (for example Fagotto *et al.*, 1999; Kishida *et al.*, 1999; Cliffe *et al.*, 2003; Schwarz-Romond *et al.*, 2007a; Faux *et al.*, 2008; Mendoza-Topaz *et al.*, 2011; Kunttas-Tatli *et al.*, 2014; Pronobis *et al.*, 2015, 2017; Thorvaldsen *et al.*, 2015).

Ubiquitination by E3 ubiquitin ligases is a key mechanism for regulating protein stability. Once the destruction complex templates βcat phosphorylation, the most N-terminal phosphorylated serine forms part of the core of a recognition motif for a Skp-Cullin-F-box (SCF)-class E3 ubiquitin ligase. This E3 ligase ubiquitinates βcat for proteasomal destruction (Jiang and Struhl, 1998; Stamos and Weis, 2013). SCF-class E3 ligases include Cullin1 (Cul1), Skp1, F-box proteins, and Ring box (RBX) subunits (Figure 1B), which work together to bind substrates and attach multiple ubiquitin moieties (Lee and Diehl, 2014). Cul1 is the scaffold of the complex, at one end binding Rbx1 and its associated E2-Ubiquitin proteins and at the other end binding Skp1. Skp1(SkpA in *Drosophila*) links Cul1 and the F-box protein—in this case, βTrCP. βTrCP (Slimb in *Drosophila*) contains the substrate recognition domain of the E3 ligase. The βcat recognition site spans the WD40 repeats on the C-terminal end of βTrCP (Wu *et al.* 2003). This domain forms a propeller structure with a pocket that binds only to phosphorylated proteins. βTrCP can bind multiple phospho-proteins and thus regulate diverse cell signaling pathways (e.g., NFκB and Hedgehog signaling). After βTrCP-βcat binding, βcat is poly-ubiquitinated and can now be recognized by the proteasome. While down-regulation of βcat levels via protein degradation is a key function of the destruction complex, our understanding of *how* βcat is transferred from the complex to the SCF E3 ligase is a key unanswered question.

Two classes of models seem plausible. In the first class of models, the E3 ligase is a physical entity separate from the destruction complex—this would fit with the many roles for the SCF^{Slimb} E3 ligase, which binds and ubiquitinates diverse phospho-proteins, ranging from the Hedgehog effector Ci/Gli to the centrosome assembly regulator PLK4 (Robertson *et al.*, 2018). However, given the abundance of cellular phosphatases, this model has a potential major problem. Phosphorylated βcat released free from the destruction complex into the cytoplasm would likely be rapidly dephosphorylated, preventing its recognition by the E3 ligase. Consistent with this, earlier work revealed that APC helps prevent βcat dephosphorylation within the destruction complex (Su *et al.*, 2008). In a second class of models, the SCF^{Slimb} E3 ligase might directly dock on or even become part of the destruction complex, either by direct interaction with destruction complex proteins or by using phosphorylated βcat as a bridge. In this model, once βcat is phosphorylated it could be directly transferred to the E3 ligase, thus preventing dephosphorylation of βcat by cellular phosphatases during transit. Immunoprecipitation (IP) experiments in animals and cell culture revealed that βTrCP can co-IP with Axin, APC, βcat, and GSK3, and that Wnt signals reduce Axin:βTrCP co-IP (Hart *et al.*, 1999; Kitagawa *et al.*, 1999; Liu *et al.*, 1999; Li *et al.*, 2012). However, these studies did not examine whether βTrCP or other components of the E3 are recruited to the destruction complex, leaving both models an option, especially if βTrCP acts as a shuttling protein between complexes. Here we address this issue.

A second set of outstanding questions concern the mechanisms by which Wnt signaling down-regulates βcat destruction. Wnt signaling is initiated when Wnt ligands interact with complex multiprotein receptors, comprised of Frizzled family members plus LRP5/6 (reviewed in DeBruine *et al.*, 2017; Nusse and Clevers, 2017). This receptor complex recruits the destruction complex to the plasma membrane via interaction of Axin with the phosphorylated LRP5/6 tail and with the Wnt effector Dishevelled (Dvl in mammals/Dsh in *Drosophila*). This leads to down-regulation of the destruction complex, reducing the rate of βcat destruction. Current data suggest destruction complex down-regulation occurs via multiple mechanisms (reviewed in MacDonald and He, 2012; Nusse and Clevers, 2017), some rapid and others initiated more slowly. These include direct inhibition of GSK3 by the phosphorylated LRP5/6 tail, inhibition of Axin homo-polymerization by competition with hetero-polymerization with Dsh, competition between Dsh and APC2 for access to Axin, targeting Axin for proteolytic destruction, and blockade of βcat transfer to the E3 ligase. In our recent work, we explored the role of Dsh. We found that overall protein levels of Axin, APC2 and Dsh in *Drosophila* embryos experiencing active Wnt signaling are within a fewfold of one another, suggesting that competition is a plausible mechanism for destruction complex down-regulation (Schaefer *et al.*, 2018). The competition model is also consistent with the effects of elevating Axin levels, which makes the destruction complex more resistant to turn-down (Cliffe *et al.*, 2003; Wang *et al.*, 2016; Schaefer *et al.*, 2018). However, somewhat surprisingly, elevating Dsh levels had only modest consequences on cell fate choices, and Dsh only assembled into Axin puncta in cells receiving Wingless signals (Wg = *Drosophila* Wnt family member; Cliffe *et al.*, 2003; Schaefer *et al.*, 2018), suggesting that Dsh may need to be "activated" by Wnt signals in order to effectively compete with APC for Axin and thus mediate destruction complex down-regulation. Candidate phosphorylation sites and kinases potentially involved in this activation have been identified (e.g., Bernatik *et al.*, 2011; Gonzalez-Sancho *et al.*, 2013; Bernatik *et al.*, 2014). Intriguingly, when Axin, APC, and Dvl were expressed in mammalian cells, potential competition between APC and Dvl for interaction with Axin was revealed (Schwarz-Romond *et al.*, 2005; Mendoza-Topaz *et al.*, 2011). Here we examined in vivo the effects of simultaneously altering levels of Dsh and Axin, testing aspects of the competition model, and combined this with analysis of how Dsh and Axin affect one another's assembly into puncta in a simple cell culture model, using structured illumination superresolution microscopy.

RESULTS

A system to examine whether the destruction complex and the SCF^{Slimb} E3 ligase colocalize

The transfer of phosphorylated βcat from the destruction complex to the E3 ubiquitin ligase to begin βcat degradation is a crucial step

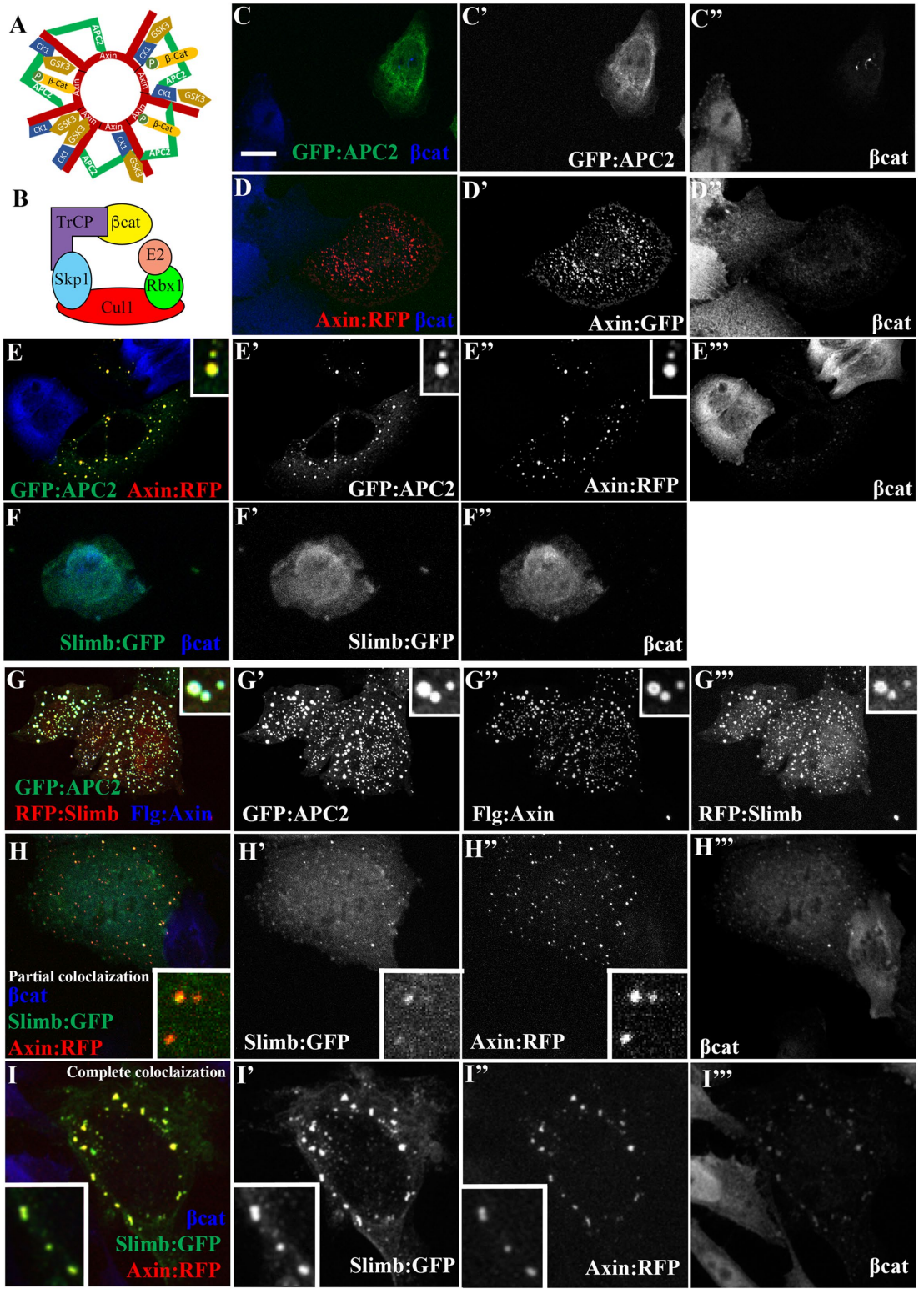

FIGURE 1: Slimb is recruited into the destruction complex by Axin. (A) Diagram illustrating components of the multiprotein destruction complex. (B) Diagram illustrating the components of the $SCF^{\beta TrCP}$ E3 ubiquitin ligase. (C–I) SW480 cells transfected with the indicated constructs encoding the *Drosophila* proteins. (C) Expression of GFP:APC2 is diffuse throughout cytoplasm and nucleus. SW480 cells lack a functional human APC and thus have high levels of βcat. Addition of *Drosophila* APC2 rescues βcat destruction. (D) Axin:RFP expressed alone forms cytoplasmic puncta due to Axin's polymerization domain. (E) When coexpressed, Axin:RFP recruits GFP:APC2 into Axin puncta. (F) When expressed alone, Slimb:GFP exhibits diffuse localization the cytoplasm and nucleus. (G) When coexpressed, GFP:APC2 and Flg:Axin can robustly recruit RFP:Slimb into puncta. (H, I) Axin:RFP can recruit Slimb:GFP into puncta. Axin:RFP either recruits a fraction of Slimb into puncta, leaving a large cytoplasmic pool of Slimb:GFP (H), or robustly recruits most of Slimb:GFP into puncta (I). Scale bar = 10 μm. Insets are higher magnification images from the same cell.

	Protein	Log_2(intensity)	Unique peptides	MS/MS counts
Destruction complex	APC	31.67	122	233
	CTNNB1	30.96	30	69
	CTNNA1	30.24	44	57
	JUP	27.29	21	25
	AMER1	27.10	21	25
	AXIN1	26.33	16	21
	GSK3B	25.39	8	11
	AXIN2	24.11	7	9
	CSNK1D/E	21.66	2	1
E3 ligase components	TRIM21	27.96	17	24
	TRIM28	24.41	7	7
	FBXW11	23.27	2	4
	SKP1	22.65	2	2
	CUL1	21.86	1	1
	MYCBP2	21.53	5	5
	CUL3	19.49	1	1
	CDC27	–	1	1

TABLE 1: Proteins identified using affinity-purification MS.

in Wnt signaling regulation, which remains incompletely understood. One key question in the field involves the mechanism by which βcat is transferred from one complex to the other. Do they each form separate structures within the cytoplasm of the cells, thus relying on either diffusion or some form of protein shuttle to move βcat between them? Or is there a "factory" for βcat destruction, containing the machinery to first phosphorylate βcat and then directly pass it down the assembly line to the E3 ligase? Previous work is more consistent with the latter model, as Axin and APC can coimmunoprecipitate (co-IP) with mammalian βTrCP (Hart *et al.*, 1999; Kitagawa *et al.*, 1999; Liu *et al.*, 1999; Li *et al.*, 2012) and one role of APC is to protect βcat from dephosphorylation before it is ubiquitinated (Su *et al.*, 2008).

We took two different approaches. For our studies, we expressed *Drosophila* proteins in mammalian cells—conservation of sequence and function means they can rescue βcat destruction in the *APC* mutant colorectal cell line SW480 (Roberts *et al.*, 2011; Pronobis *et al.*, 2015; Figure 1, C–E). *Drosophila* APC2 is also half the size of human APC1 and therefore easier to transfect and express in cells. First, we examined recruitment of E3 ligase components using mass spectroscopy. We used affinity-purification mass spectrometry (AP/MS) to pull down Flag-tagged *Drosophila* APC2 that had been stably expressed in human HEK293T cells. Mass spectroscopy analysis identified the known core components of the destruction complex including βcat, alpha-catenin, GSK3, CK1, Axin1, and Axin2, as well as other proteins previously identified to interact with the destruction complex by mass spectroscopy (e.g., WTX/AMER1, plakoglobin, USP7, and CTBP; Major *et al.*, 2007; Hilger and Mann, 2012; Li *et al.*, 2012). Our list also included a number of components of different E3 ligases, including the three core components of the SCF^{TrCP} E3 ligase (known destruction complex proteins and components of E3 ligases are summarized in Table 1, while the full mass spectroscopy dataset is presented in Supplemental Table S1). Using the label-free quantification (LFQ) intensity as a measure for quantification, our data were consistent with the following hierarchical order: FBXW11 = βTrCP2 > SKP1 > Cul1. However, the recovery of these proteins was less robust than that of the core destruction complex proteins. βTrCP2 and Skp1 were also identified in previous mass spectroscopy analysis with Axin as a bait, and Skp1 was also identified in APC pull downs (Hilger and Mann, 2012). These data are consistent with the possibility that the SCF^{Slimb} E3 ligase is recruited, at least transiently, to the destruction complex.

To further explore βcat transfer to the E3 ligase, we transfected components of the destruction complex and of the E3 ligase into SW480 colorectal cancer cells to determine whether they colocalize, thus suggesting recruitment of the E3 ligase to the destruction complex. To visualize the destruction complex, we tagged *Drosophila* Axin or APC2 with GFP, RFP, or Flag epitope tags (Roberts *et al.*, 2011; Pronobis *et al.*, 2015). When GFP-tagged APC2 (GFP:APC2) is transfected in cells alone, APC2 is found throughout the cytoplasm (Roberts *et al.*, 2011; Figure 1C). In contrast, when RFP-tagged Axin is transfected alone (Axin:RFP), it forms cytoplasmic puncta due to Axin's ability to self-polymerize via its DIX domain (Figure 1D; Kishida *et al.*, 1999). Finally, when GFP:APC2 is expressed along with Axin:RFP, GFP:APC2 is recruited into Axin puncta (Roberts *et al.*, 2011; Figure 1E). Previous studies revealed that this APC2-Axin interaction leads to larger, stabilized destruction complexes (Kunttas-Tatli *et al.*, 2014; Pronobis *et al.*, 2015). We note that while we include βcat images in some panels, our goal in this set of experiments was to assess recruitment of E3 ligase proteins to the destruction complex, not assess their impact on restoring βcat destruction to these *APC* mutant SW480 cells, and thus we did not carry out quantitative analysis of βcat levels.

We next assessed whether Slimb has any specific localization pattern on its own in SW480 cells. We tagged *Drosophila* Slimb with GFP, RFP, or Flag tags. When Slimb was expressed alone, it was diffusely localized in both the cytoplasm and the nucleus, without obvious enrichment in any subcellular structure (Figure 1F), and Slimb expression alone had no apparent effect on βcat levels. In a few cells, there was slight enrichment of Slimb in puncta near the

nucleus, which may be due to the SCF^{Slimb} E3 ligase's known role in regulating centrosome duplication (Wojcik *et al.*, 2000). This system thus provided a platform to examine whether different components of the SCF^{Slimb} E3 ligase are recruited to the destruction complex

Axin can recruit Slimb into the destruction complex while APC2 does not

Previous studies revealed that Axin and APC can co-IP with βTrCP (Hart *et al.*, 1999; Kitagawa *et al.*, 1999; Liu *et al.*, 1999; Li *et al.*, 2012), and βTrcP2 was identified in complex with Axin by mass spectroscopy (Hilger and Mann, 2012). We first examined whether this interaction was sufficient to recruit the βTrCP homologue Slimb into destruction complex puncta. When we coexpressed both Flag:Axin and GFP:APC2 with an RFP-tagged Slimb, Slimb was robustly recruited to Axin/APC puncta (Figure 1G). However, this did not discriminate whether Axin or APC recruited Slimb.

When APC was first discovered, it was believed to be the scaffold of the destruction complex, as it binds βcat and co-IPs with the kinase GSK3 (Polakis, 1997). However, subsequent work revealed that Axin is the actual destruction complex scaffold, mediating complex assembly by directly binding all core destruction complex components: APC, GSK3, CK1, and βcat (Spink *et al.*, 2000; Liu *et al.*, 2002; Dajani *et al.*, 2003). To define whether APC and/or Axin can recruit Slimb, we coexpressed Axin plus Slimb or APC2 plus Slimb. The ability of Axin to form puncta made examining Slimb recruitment straightforward. Coexpression of RFP-tagged Axin (Axin:RFP) with GFP-tagged Slimb (Slimb:GFP) revealed that Axin robustly recruits Slimb:GFP into cytoplasmic puncta (Figure 1, H and I and close-up insets; 135/140 cells examined; Table 2). The degree of Slimb:GFP recruitment into Axin:RFP puncta varied from Slimb enrichment in puncta with a remaining cytoplasmic pool (Figure 1H; 94/140 cells; Table 2) to nearly complete recruitment into puncta (Figure 1I; 41/140 cells; Table 2). While Axin puncta number varied from experiment to experiment (e.g., Figure 1, D vs. E; G vs. H), likely due to differences in transfection efficiency, we did not see any systematic variation in Axin puncta number that correlated with Slimb coexpression. Thus Axin has the ability to recruit Slimb.

Since APC2 has no specific localization pattern when expressed on its own (Figure 1C), it is difficult to assess whether APC2 can recruit other proteins. We therefore utilized an APC2 construct containing a mitochondrial localization signal (mito:APC2; Roberts *et al.*, 2012). Mito:APC2 is readily recruited to the mitochondria and remains functional, as evidenced by the reduction of βcat levels in SW480 cells and the ability to rescue *Drosophila* APC2 mutants (Figure 2A; Roberts *et al.*, 2012). Mito:APC2 can effectively recruit exogenous Axin (Figure 2B; Roberts *et al.*, 2012). We therefore expressed GFP-tagged mito:APC2 with RFP-tagged Slimb to test whether APC2 can recruit Slimb. Mito:APC2 was unable to detectably recruit Slimb (Figure 2C; 0/10 cells examined), consistent with the idea APC2 does not directly interact with this E3 ligase component. This is consistent with previous work demonstrating that co-IP of βTrCP2 and APC required coexpression of Axin (Kitagawa *et al.*, 1999). It is worth noting that since mito:APC can restore destruction of βcat, it must also recruit low levels of endogenous Axin, but these do not appear to be sufficient to efficiently recruit Slimb.

Recruitment of other SCF^{Slimb} E3 ligase components by Axin is substantially less robust

We next explored whether the other SCF^{Slimb} E3 ligase proteins, SkpA or Cul1, are recruited into the destruction complex. To test this, we coexpressed Axin:RFP with either GFP-tagged Cul1 (GFP:Cul1) or GFP-tagged SkpA (GFP:SkpA). When expressed alone, both SkpA and Cul1 were found throughout the cytoplasm and nucleus (Figure 3, A and B) and did not trigger any obvious reduction in βcat levels. We were surprised to find that while Slimb was robustly recruited to Axin puncta (Figure 1, H and I; Table 2), Cul1 and SkpA were not. For SkpA there was no recruitment in 48/52 cells examined (Figure 3C; Table 2), and for Cul1 we observed no recruitment in 36/42 cells examined (Figure 3D; Table 2). When colocalization was observed for SkpA or Cul1, it was minimal (Figure 3C inset; Table 2). Consistent with previous work with the mammalian homologues, we could co-IP Axin with Slimb (Figure 3, E′, lane 2, and F′, lane 2), but did not detect robust co-IP of APC2 with Slimb (Figure 3E′, lane 3). Similarly, we did not detect co-IP of Axin with either Cul1 or SkpA (Figure 3F′, lanes 3 and 4). These data suggest that Axin can recruit Slimb to the destruction complex but is unable to strongly recruit the other components of the E3. We also examined whether Slimb recruitment into Axin puncta stimulated recruitment of other SCF^{Slimb} E3 ligase proteins. To do so, we coexpressed Axin, Slimb, and SkpA—in this case we saw modest corecruitment of Slimb and SkpA to Axin puncta in a small subset of cases (3/20 cells; Figure 3G and insets); however, 17/20 cells showed no SkpA recruitment. Together these data are consistent with the idea that

Proteins examined	No colocalization	Partial colocalization	Complete colocalization	Total number of cells analyzed	Number of experiments
Axin + Slimb	5	94	41	140	17
Axin + SkpA	48	4	0	52	6
Axin + Cul1	36	6	0	42	6
AxinΔRGS + Slimb	23	4	0	27	6
AxinΔβcat + Slimb	0	6	13	19	4
SrtAftRGS + Slimb	7	3	0	10	3
Axin + NTerm-Slimb	15	34	1	50	7
Axin + CTerm-Slimb	18	26	7	51	7

Summary of Axin's ability to recruit E3 Ligase components. Genes encoding the wild-type or mutant proteins indicated were transfected into SW480 cells. No colocalization, no recruitment of protein into Axin puncta. Partial localization, protein recruited into a subset of puncta with substantial levels remaining in the cytoplasm. Complete colocalization, all Axin puncta have recruited its partner protein into the puncta, and cytoplasmic levels are reduced. Total number of cells analyzed represents cells imaged. The number of experiments equals the number of independent times cells were transfected with the labeled protein combinations.

TABLE 2: Summary of Axin's ability to recruit E3 ligase components.

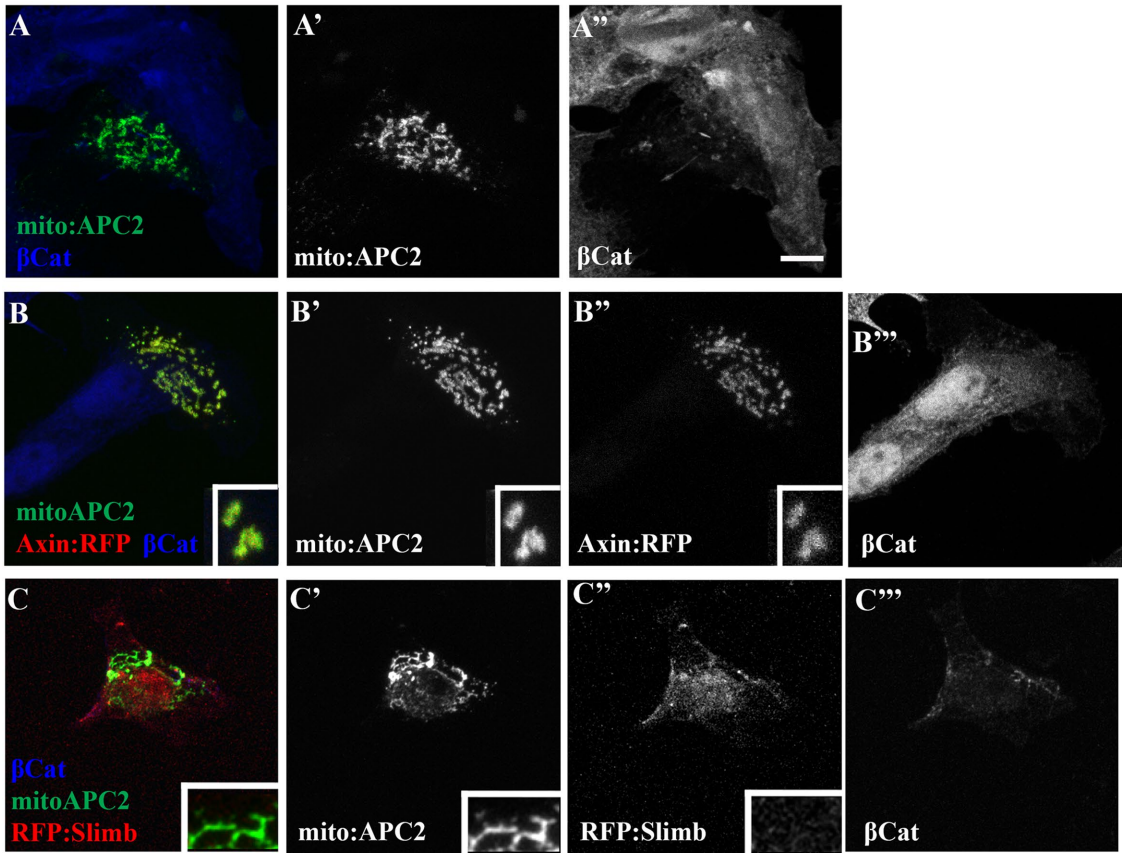

FIGURE 2: APC2 is unable to recruit Slimb. (A–C) SW480 cells transfected with the indicated constructs. (A) Expression of GFP-tagged APC2 fused in frame to a mitochondrial localization signal (mito:APC2). Even though APC2 is immobilized at the mitochondrial membrane, it is still able to enhance βcat destruction. (B) Mito:APC2 coexpressed with Axin:RFP. Mito:APC2 is able to recruit Axin:RFP. (C) Mito-APC2 expressed with RFP:Slimb. RFP:Slimb was not recruited by APC2. Scale bar = 10 μm. Insets are higher magnification images from the same cell.

Slimb is robustly recruited to the destruction complex via direct or indirect interaction with Axin, and that other E3 ligase components (SkpA and Cul1) are less robustly recruited.

Axin's RGS domain is required for efficient Slimb recruitment but its βcat-binding domain is not

Both Axin and Slimb directly bind to βcat, but at different locations on βcat (Xu and Kimelman, 2007). Therefore, some studies suggested that the Axin:Slimb interaction in vivo may not be direct, but instead might be mediated via bridging by βcat (Liu *et al.*, 1999), or at least be enhanced by this (Kitagawa *et al.*, 1999). APC2 is also able to directly bind to βcat. If Axin solely recruits Slimb via a βcat linker, then APC2 should also be able to recruit Slimb, something that is not supported by our data (Figures 2C and 3, E and E'). To further test the hypothesis that Axin recruits Slimb via a βcat bridge, we used an Axin mutant lacking the βcat-binding site (AxinΔβcat:RFP; Figure 4A; Pronobis *et al.*, 2017) and coexpressed it with Slimb. If βcat is essential as a bridge between Slimb and Axin, we would expect this Axin mutant to no longer recruit Slimb into Axin puncta. In contrast, if Axin and Slimb can also interact by another means, then Slimb should still be recruited into the puncta. When AxinΔβcat:RFP was expressed alone, it formed cytoplasmic puncta, consistent with the fact that it still contains Axin's self-polymerization DIX domain (Figure 4C), though it is unable to target βcat for destruction (Pronobis *et al.*, 2017). Strikingly, when coexpressed with Slimb:GFP, AxinΔβcat:RFP was still able to robustly recruit Slimb:GFP into puncta (Figure 4F; 19/19 cells showed recruitment; Table 2), suggesting that the Slimb–Axin interaction is not solely a result of both proteins binding to βcat.

To further investigate which domain(s) of Axin are required for Slimb recruitment, we used two additional mutants of Axin deleting other domains or regions (Figure 4A; Pronobis *et al.*, 2017): 1) AxinΔRGS:RFP removed the RGS domain, which is one of the Axin:APC interaction sites (Spink *et al.*, 2000), and 2) Start After RGS:RFP, which lacks the N-terminal third of Axin. Both mutants retained the ability to form puncta (Figure 4, D and E; Pronobis *et al.*, 2017). Each RFP-tagged Axin mutant was then coexpressed with GFP-tagged Slimb. Both mutants lacking the RGS domain, AxinΔRGS:RFP and Start After RGS:RFP, were diminished in their ability to robustly recruit GFP:Slimb (Figure 4, G and H; AxinΔRGS = 23/27 cells showed no recruitment; Start After RGS = 7/10 cells showed no recruitment; and in those cells where colocalization was observed, it was partial; Table 2). To test this interaction in another way, we IPed Axin mutants tagged with RFP and assessed if Slimb was co-IPed. Full-length Axin, AxinΔβcat:RFP, and AxinΔDIX:RFP (Axin lacking its self-polymerization domain; Figure 4A) were all able to co-IP Slimb (Figure 4, B1 and B2). However, the two Axin mutants lacking the RGS domain did not effectively co-IP with Flag:Slimb (Figure 4, B1 and B2; the reduced ability of Slimb to co-IP with AxinΔRGS was seen in three of three replicates). These data suggest that the RGS domain helps mediate the Axin–Slimb interaction.

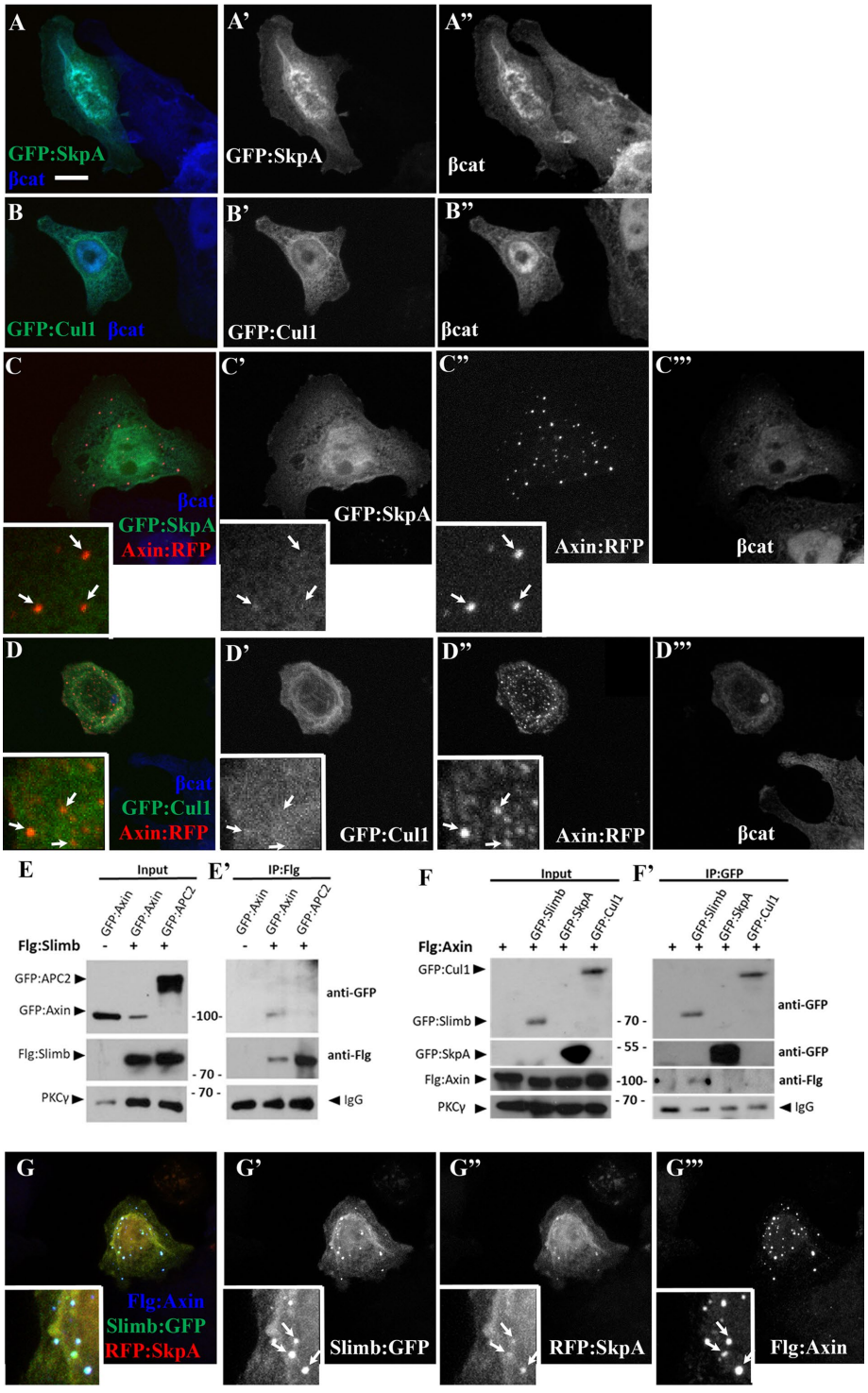

FIGURE 3: Axin does not recruit Cul1 or SkpA into the destruction complex. (A–D, G) SW480 cells transfected with the indicated *Drosophila* proteins. (A, B) GFP-tagged SkpA and Cul1 both accumulate throughout the cytoplasm and nucleus and their expression does not appear to affect βcat destruction. (C, D) Cotransfection of Axin:RFP with either GFP:SkpA (C) or Cul1 (D). Axin is unable to robustly recruit either SkpA or Cul1. (E) Testing whether GFP-tagged APC2 or Axin co-IP with Flg-tagged Slimb. Slimb co-IPs with Axin and not APC2. (F) Testing whether Flg-tagged Axin co-IPs with GFP-tagged forms of E3 ligase protein. Flg:Axin co-IPs with Slimb but not with SkpA or Cul1. All blots are from the same gel, with extraneous lanes removed. (G) Coexpression of Flg:Axin, Slimb:GFP, and RFP:SkpA. Axin is able to robustly recruit Slimb but is less efficient at recruiting SkpA, insets. Arrows point to the same punctum in each channel. Scale bar = 10 μm. Insets are higher magnification images from the same cell.

Slimb recruitment into the destruction complex can be mediated by either the N-terminal or the C-terminal regions of the protein

We similarly asked which part of the multidomain Slimb protein is required for recruitment. We divided Slimb protein roughly in half, separating the N-terminal F-box, which binds SkpA, from the C-terminal WD40 repeats, which dock substrate (Figure 5A). When expressed alone, both halves localized throughout the cytoplasm and nucleus (Figure 5, B and D). Strikingly, both halves could be recruited to Axin puncta (Figure 5, C, E, and F, arrows in insets), though neither was as robustly recruited as full-length Slimb (the N-terminal half was recruited into Axin puncta in 35/50 cells, and the C-terminal half was recruited into Axin puncta in 34/51 cells, while recruitment of full-length Slimb was seen in 135/140 cells, and partial colocalization [Figure 5F] was more common with the Slimb fragments; Table 2). These data suggest a multipartite binding interaction, consistent with earlier assessment by co-IP (Kitagawa *et al.*, 1999).

Slimb is a dynamic component of the destruction complex

The destruction complex has many of the properties of a biomolecular condensate (Schaefer and Peifer, 2019). One of these is the ability of individual components to rapidly exchange with the cytoplasmic pool—Axin, APC2, and Dsh can all move into and out of puncta (Schwarz-Romond *et al.*, 2005; Kunttas-Tatli *et al.*, 2014; Pronobis *et al.*, 2015). This property can be measured using fluorescence recovery after photobleaching (FRAP), in which fluorescently tagged protein components of a protein complex are photobleached, and exchange with the unbleached cytoplasmic pool is assessed. FRAP analysis provides an assessment of the mobile fraction (the total amount of protein turnover at the recovery plateau). For example, if there were 100 GFP-tagged proteins in a punctum, and we observed 30% recovery of the total GFP fluorescence, this would suggest that on average 70 proteins remained in the complex and 30 new proteins entered. FRAP also provides an assessment of the half-time of recovery ($t_{1/2}$), the amount of time necessary to replace half of the total recovered fluorescence. This measure provides turnover rate. Previous analysis revealed that when expressed alone, Axin:RFP is relatively mobile; however, when Axin is coexpressed with APC2, FRAP recovery is less complete and takes significantly longer (Pronobis *et al.*, 2015). These data suggested that APC2 stabilizes Axin assembly into puncta. In contrast,

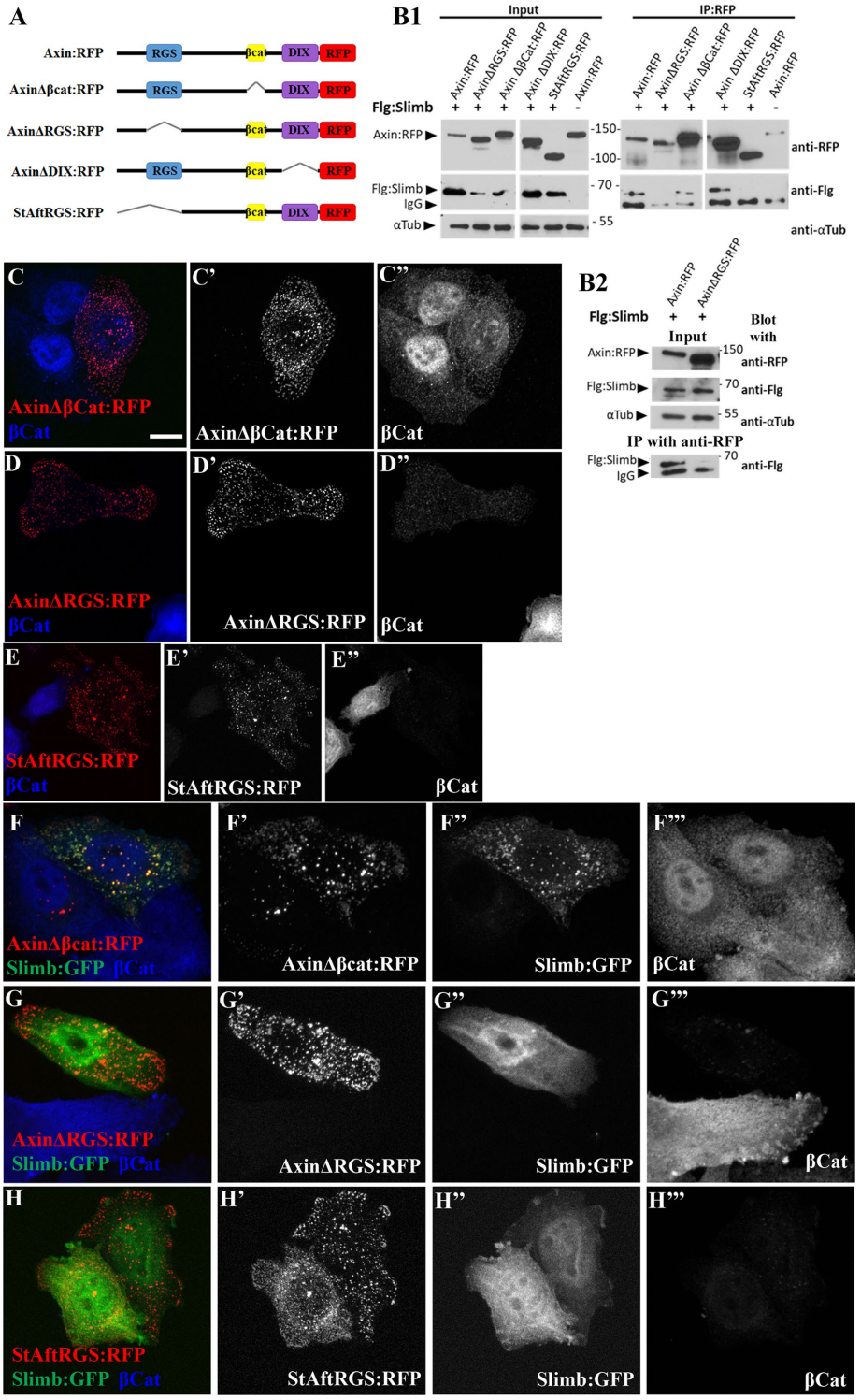

FIGURE 4: The RGS domain of Axin enhances Slimb recruitment into Axin puncta while the βcat-binding site is not essential. (A) Diagram of different Axin mutant constructs used. (B1, B2) Testing whether Flag-tagged Slimb co-IPs with different RFP-tagged Axin mutants. Axin constructs missing the RGS domain do not co-IP with Slimb. B1 and B2 are independent replicates. Within B1 all blots are from the same gel, with nonrelevant lanes removed. (C–H) Expression in SW480 cells of different Axin mutants, as indicated, alone (C–E) or with Slimb:GFP (F–H). Only AxinΔβcat:RFP is able to robustly recruit Slimb into puncta. Scale bar = 10 μm.

Dsh coexpression increases Axin exchange (Schwarz-Romond *et al.*, 2007b). To gain an understanding of Slimb dynamics in the destruction complex and the effect of APC2 on its dynamics, we first coexpressed Axin:RFP and GFP:Slimb. Slimb behaved as a dynamic component of the destruction complex (Figure 6, A and C). Its recovery plateau was ~50% and it had a $t_{1/2}$ of ~100 s (Figure 6, D and E). In contrast to Axin, Slimb dynamics were not significantly altered when puncta included both Axin and APC2 (Figure 6, B–E), suggesting that stabilization of Axin by APC2 does not stabilize Slimb in the destruction complex. These data support the idea that Slimb can form a complex with Axin but is readily able to move out of this complex, consistent with the possibility that Slimb shuttles βcat between the destruction complex and the E3 ligase.

Slimb localizes along Axin polymers within destruction complex puncta

To further investigate the Axin:Slimb interaction, we visualized this complex by structured illumination microscopy (SIM), which allows increased resolution. When Axin:RFP is expressed alone, puncta contain small circular polymers of Axin, presumably assembled by DIX domain polymerization, as we and others previously observed (Figure 6, F, G1, and G2 arrows; Pronobis *et al.*, 2015; Thorvaldsen *et al.*, 2015). In contrast, after coexpression of GFP:APC2 with RFP:Axin, APC2 and Axin form intertwined polymers, with an increase in Axin polymer size/complexity (Figure 6, H, H1, arrow, and I; Pronobis *et al.*, 2015). To explore the relationship of Axin and Slimb within the destruction complex, we coexpressed Axin:RFP and Slimb:GFP (Figure 6J). At the level of the whole cell, Slimb and Axin colocalized in puncta (Figure 6J) and the addition of Slimb did not obviously alter average Axin puncta size or number. Unlike what we previously observed with APC2 (Pronobis *et al.*, 2015), Slimb coexpression did not have an obvious effect on Axin polymer structure—Axin continued to form circular polymers along which Slimb and Axin largely colocalized with some variations in intensity (Figure 6, J1 and K, arrows) These data are consistent with the idea that Axin forms a scaffold on which Slimb localizes. Together with the data above, these experiments further our understanding of the mechanisms by which βcat is transferred from the destruction complex to the E3 ligase, thus ensuring its ultimate destruction.

Exploring how Dsh, Axin, and APC cooperate and compete to modulate Wnt signaling in vivo

The data above help illuminate how a functional destruction complex and E3 ligase cooperate to mediate βcat destruction. Wnt signaling can turn down this process, stabilizing βcat and allowing it to enter the nucleus and help activate transcription. We thus next turned to

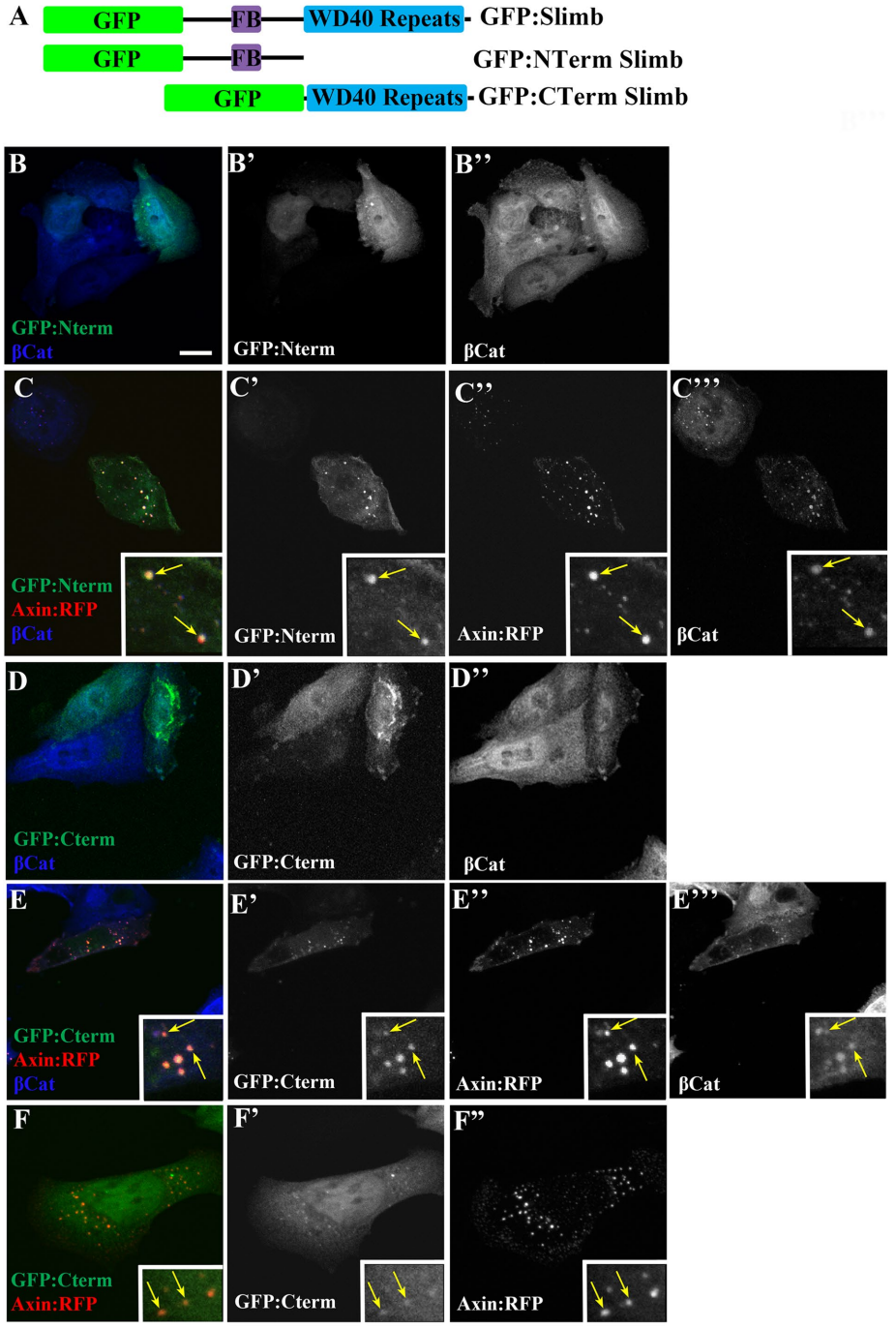

FIGURE 5: Both halves of Slimb can be recruited by Axin. (A) Diagram of the Slimb constructs used. The N-terminal half contains the F-box domain (FB) which mediates binding to SkpA. The C-terminal half consists mostly of the WD40 repeat domain, which binds to Slimb substrates. (B, D) Both GFP-tagged portions of Slimb localize throughout the cytoplasm and nucleus when expressed alone, and neither has a strong effect on βcat levels. (C, E, F) Cotransfection of either Slimb fragment with Axin:RFP reveals that both can be recruited to Axin puncta (C, E, F inset arrows), although the degree of recruitment varies (E vs. F). Insets are higher magnification images from the same cell. Scale bar = 10 μm.

exploring mechanisms underlying this. Cell fate choice in the *Drosophila* embryonic epidermis provides one of the best in vivo models for regulation of Wnt signaling. The GAL4-UAS system likewise offers a superb toolkit to modulate levels of proteins involved in the signaling cascade (Brand and Perrimon, 1993; Duffy, 2002). Using different combinations of GAL4 drivers and UAS constructs allows titration of protein levels over a wide range. We and others have used this system to probe mechanisms underlying the function of the destruction complex and its down-regulation by Wnt signaling.

Coassembly of Axin and APC is critical to build a functional destruction complex in vivo (e.g., Mendoza-Topaz *et al.*, 2011). Wnt signaling triggers down-regulation of the destruction complex, and the ability to do so depends on relative Axin levels. Thus, while a three- to fourfold increase in Axin levels is tolerated by the developing embryo (Wang *et al.*, 2016; Schaefer *et al.*, 2018), more substantial increases in Axin levels prevent inactivation of the destruction complex even in cells exposed to the Wnt ligand (Willert *et al.*, 1999; Cliffe *et al.*, 2003; Schaefer *et al.*, 2018). Dsh is a key positive effector of Wnt signaling and its ability to homopolymerize and to heteropolymerize with Axin are critical for down-regulating the destruction complex (Schwarz-Romond *et al.*, 2007a,b; Fiedler *et al.*, 2011; Mendoza-Topaz *et al.*, 2011). Work in cultured cells suggests Dsh can compete with APC for association with Axin, providing a potential mechanism for Dsh's role in destruction complex down-regulation (Fiedler *et al.*, 2011; Mendoza-Topaz *et al.*, 2011). Surprisingly, in *Drosophila* embryos elevating Dsh levels sevenfold has only modest effects on viability and cell fate choices (Cliffe *et al.*, 2003; Schaefer *et al.*, 2018), suggesting that Dsh may need to be "activated" by Wnt signaling in order to compete for Axin binding.

Surprisingly, elevating Dsh levels can potentiate the ability of Axin to inhibit Wnt signaling

The simplest versions of the competition hypothesis would predict that elevating Dsh levels would blunt the effects of elevating Axin levels. To test this, we varied the absolute and relative levels of Axin and Dsh. Previous work suggested competition between APC and Dsh for Axin occurs in vivo (Cliffe *et al.*, 2003), but those experiments did not assess relative levels of misexpression and also did not control for the potential quenching effect on Axin overexpression of driving more than one UAS/Gal4 construct in the same embryo. Our recent work provided misexpression tools allowing us to control for both these variables and provide quantitative assessments of relative levels of the two proteins under different conditions (Schaefer *et al.*, 2018). We used a strong maternal GAL4 driver line to create robust, uniform, and early maternal and zygotic expression of one transgene (either a GFP-tagged Axin [Axin:GFP] or a Myc-tagged Dsh [Dsh:Myc]) and expressed the other UAS construct zygotically to allow us to modulate the ratios of

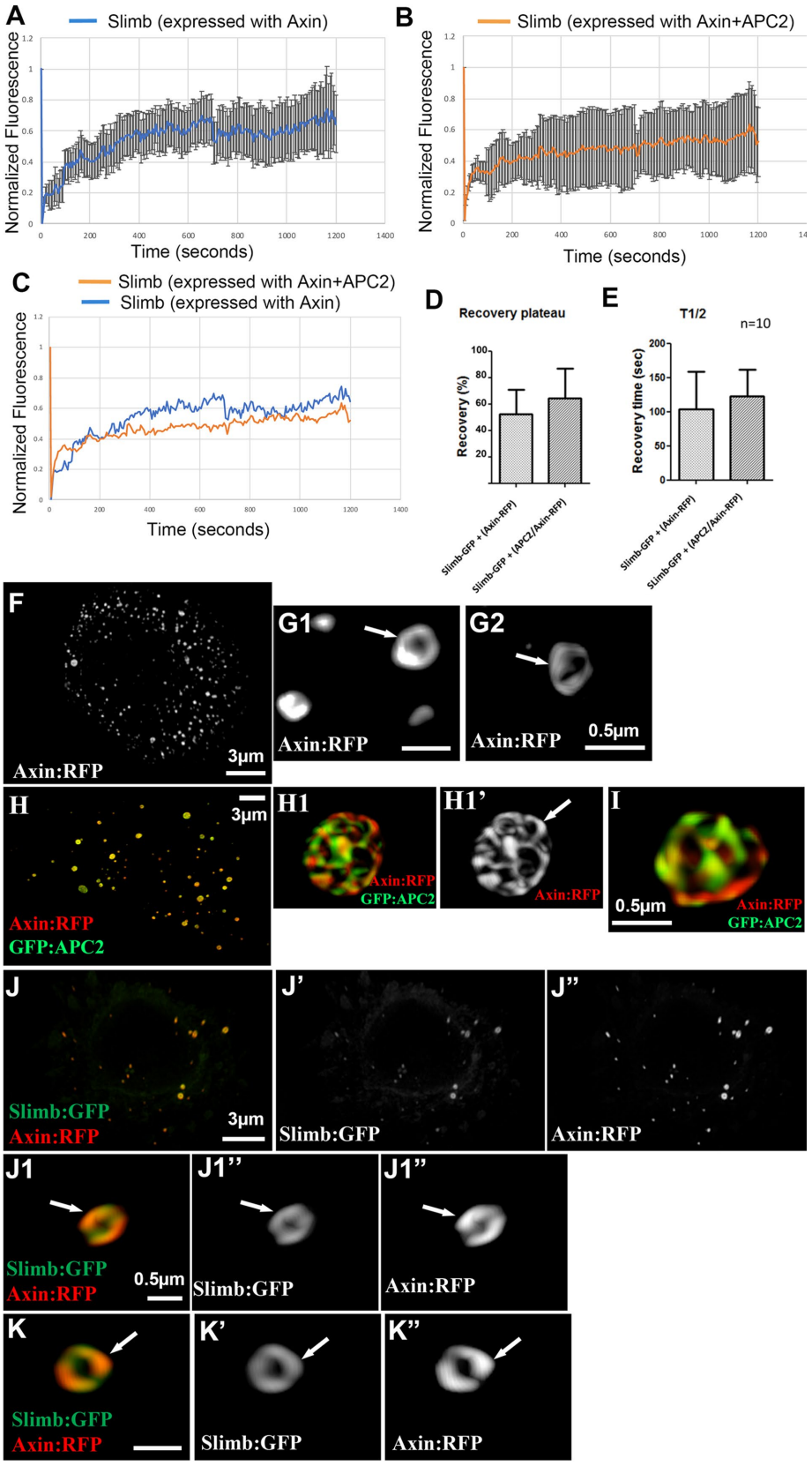

FIGURE 6: Slimb is a dynamic component of the destruction complex, the turnover of which is not affected by coexpression with APC2, and SIM imaging reveals that Slimb is recruited along Axin polymers. (A, B) Slimb:GFP FRAP recovery curves when coexpressed with RFP:Axin (A) or with both RFP:Axin and Flag-tagged APC2. Error bars indicate standard errors out of 10 puncta (1 punctum per cell). (C) Recovery curves are similar after coexpression with Axin or with Axin plus APC2. (D, E) Slimb mobility in puncta is unchanged when expressed with Axin vs. APC2 and Axin and Dsh. We also used a UAS-RFP construct to control for the effects of multiple GAL4 driven transgenes. (F–K) SIM of SW480 cells expressing the indicated constructs, which were directly imaged via the fluorescent tag. (F, H, J) SIM images of whole cells. Scale bar = 3 μm. (G1, G2, H1, I, J1, K) Close-up images. Scale bar = 0.5 μm. (G1, G2) Axin expressed alone assembles into tight circular polymers. (H1, I) APC2 coexpression increases the size and complexity of Axin puncta, revealing intertwined polymers of Axin and APC2, as we previously observed (Pronobis *et al.*, 2015). (J1, K) Close-ups of puncta in cells expressing both Slimb:GFP and Axin:RFP. Slimb closely localizes with Axin polymers. J1 is a close-up of a punctum from J; K is from another cell.

We first assessed effects on embryonic viability and cell fate choice. When wild-type embryos secrete cuticle, anterior cells within each segment produce denticles and posterior cells naked cuticle (Figure 7B, middle). Constitutive activation of Wnt signaling converts cells to naked cuticle fates (Figure 7B, left) while inactivating Wnt signaling expands denticle cell fates (Figure 7B, right). We used cell fate scoring criteria that we previously developed to assess this Wnt activation or inactivation (Figure 7C; Schaefer *et al.*, 2018). As we previously found, mild zygotic Axin overexpression (Mat>RFP x Axin; twofold increase in Axin levels; Schaefer *et al.*, 2018; crosses used and cross nomenclature are in *Materials and Methods*) had little or no effect on embryonic viability (Figure 7A) or cell fate choices, as assessed by cuticle pattern (Figure 7C). In contrast, stronger maternal/zygotic Axin overexpression (Mat>Axin x Axin; ninefold increase in Axin levels; Schaefer *et al.*, 2018) substantially reduced embryonic viability (Figure 7A) and suppressed Wg-dependent cell fates, thus reducing naked cuticle (Figure 7C; Schaefer *et al.*, 2018). In contrast, increasing levels of Dsh sevenfold (Mat>Dsh x Dsh; Schaefer *et al.*, 2018) had only modest effects on embryonic viability (Figure 7A) or cell fate choice (Figure 7C)—expanded naked cuticle is the cell fate expected for a positive Wnt effector.

If Dsh competes with APC for access to Axin, we hypothesized that Dsh overexpression should blunt the effects of Axin overexpression. To make it more likely that Dsh levels would be sufficiently high to effectively compete with Axin, we expressed Dsh maternally and brought Axin in zygotically (Mat>Dsh x Axin). We first

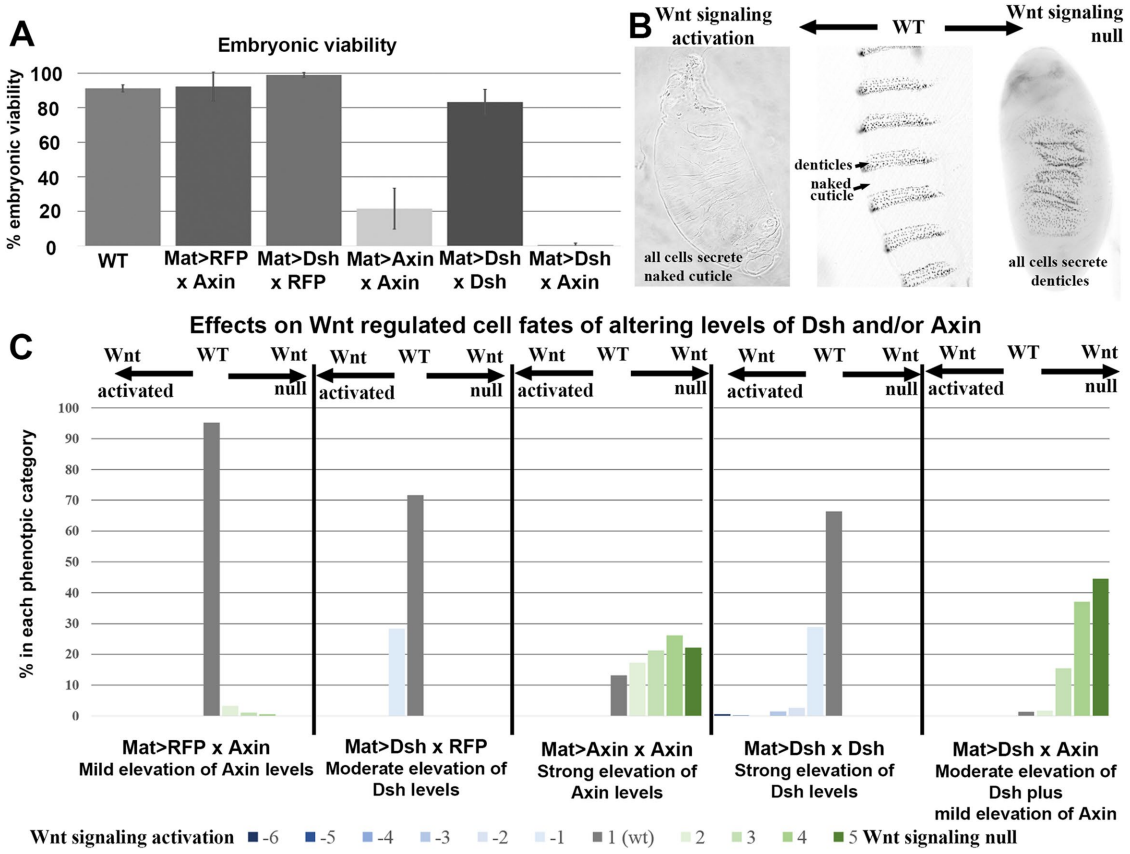

FIGURE 7: Elevating Dsh levels enhances the ability of Axin to inhibit Wg signaling. (A) Embryonic viability of indicated genotypes. See *Materials and Methods* for more details on genotype abbreviations; *n* = 283, 490, 424, 237, 374, and 421 embryos, respectfully. (B) Representative images of wild type (center), with segmentally repeated denticle belts and naked cuticle, flanked by the two most extreme cuticle phenotypes. The left image represents Wnt signaling hyperactivation, which results in loss of denticle belts, leaving behind naked cuticle. This is equivalent to phenotype –6 in C. The right image illustrates strong loss of Wnt signaling, inducing loss of naked cuticle and merging of denticle belts. This is equivalent to phenotype 5 in C. (C) Range of cuticle phenotypes observed in dead embryos and hatched larva of genotypes is indicated. Categories are as described in Schaefer *et al.* (2018). Briefly: –6 = Naked cuticle with no denticle belts and large head hole; –5 = naked cuticle with smaller head hole; –4 = small head hole with patches of denticle; –3 = less than ½ of total denticles remain; –2 = more than ½ of denticle are still present, head appears normal; –1 = at most 1 full or parts of 2 denticle belts are absent; 1 = wild-type cuticle phenotype with alternating naked cuticle and denticle belts; 2 = 1–2 merged denticle belts; 3 = 3–4 merged denticle belts; 4 = most denticle belts are merged but mouth parts are still present; and 5 = merged denticle belts with no head.

examined embryonic viability and effects on cell fate choice, as assessed by examining cuticle phenotypes. Maternal expression of Dsh alone (Mat>Dsh x RFP) had no effect on embryonic viability (Figure 7A) and only modest effects on cell fate choice, reflecting occasional mild activation of Wnt signaling (Figure 7C). However, when we combined maternal expression of Dsh with zygotic expression of Axin (Mat>Dsh x Axin), the result was quite unexpected. This led to essentially complete embryonic lethality (Figure 7A) and strong suppression of Wnt signaling, as assessed by cuticle pattern (Figure 7C), the opposite of what we predicted. In fact, the effect on cell fate choice was as strong or stronger than that seen with high-level maternal and zygotic expression of Axin (Mat>Axin x Axin, Figure 7C). In contrast, the relatively low-level zygotic expression of Axin alone (Mat>RFP x Axin; Figure 7C) did not affect embryonic viability and only occasionally caused mild inhibition of Wnt signaling. This suggested that elevating Dsh levels can potentiate the ability of Axin to inhibit Wnt signaling.

Elevating Dsh levels can enhance the ability of Axin to target Arm for destruction

The direct target of the destruction complex is Armadillo (Arm), the *Drosophila* homologue of βcat. In wild-type embryos, a single row of cells in each segment expresses the Wnt ligand Wg, which moves across the segment, leading to a graded level of signaling (Figure 8, A and B). All cells have a pool of Arm at the plasma membrane, bound to E-cadherin to function in βcat's other role in adherens junctions. However, in cells that do not receive Wg signal, the destruction complex captures most of the remaining Arm and targets it for destruction, thus creating a graded distribution of cytoplasmic/nuclear Arm across the segment, with highest levels centering on the Wg-expressing cells and lowest levels at the most distant cells from the Wg source (Figure 8, A and B). To directly assess how altering the relative ratios of Axin and Dsh affect Arm levels, we examined the Arm accumulation in stage 9 embryos, in which Wg signaling is most active. In wild-type embryos, cell rows expressing Wg and Wg-adjacent cell rows have elevated cytoplasmic/nuclear

Arm levels (Figure 8B, red arrowheads), while cells farthest from Wg-expressing cells have low cytoplasmic/nuclear levels of Arm. We quantified these levels by measuring Arm fluorescence intensity in two groups of cells (as in Schaefer *et al.*, 2018): 1–2 cell rows centered on cells expressing Wg (the Wg stripes) and 1–2 cell rows farthest from the Wg-expressing cells (the interstripes). We quantified both relative Arm levels in stripes (Figure 8A, pink bars, Figure 8B, red arrowheads) versus interstripes (Figure 8A, black arrows; quantification in Figure 8G) and also the difference in levels between these populations (Figure 8A, red arrow; quantification in Figure 8H).

In wild type, this analysis clearly revealed the stabilization of Arm by Wg signaling in stripe versus interstripe cells (Figure 8, B, G, and H). In contrast, high-level expression of Axin (Mat>Axin x Axin) reduced Arm levels in the Wg stripes (Figure 8D) and thus essentially abolished the difference in levels (Figure 8, G and H; $p < 0.0001$), as we previously observed (Schaefer *et al.*, 2018). In contrast, mild zygotic elevation of Axin levels (Mat>RFP x Axin) had little or no effect on Arm levels (Figure 8, C, G, and H). However, the same modest elevation of Axin levels had striking effects in embryos that also overexpressed Dsh (Mat>Dsh x Axin)—Arm levels were reduced in cells receiving Wnt signaling (Figure 8, F and G), thus significantly reducing the difference in Arm accumulation between Wnt-ON and Wnt-OFF cells relative to wild type (Figure 8H; $p < 0.0001$). This resembled the effect of much higher elevation of Axin in embryos not overexpressing Dsh (Figure 8, D, G, and H; Mat>Axin x Axin) and contrasted with the effects of expressing low levels of Axin alone without elevating Dsh levels (Figure 8, C, G, and H; Mat>RFP x Axin). As a control, we verified that elevating Dsh levels alone did not significantly disrupt Arm stabilization in Wnt-ON cells or Arm destruction in Wnt-OFF cells (Figure 8, E, G, and H). Thus, elevating Dsh levels enhances the ability of Axin to target Arm for destruction in cells receiving Wnt signals, contrary to our original hypothesis.

As a final assessment of the effect on Wnt signaling of elevating both Dsh and Axin levels, we examined the expression of the protein encoded by a Wnt target gene, *engrailed* (*en*). In a wild-type embryo, the two most posterior rows of cells in each segment express Engrailed (En; Figure 8, I and N), and maintenance of this expression requires Wnt signaling (DiNardo *et al.*, 1988). To assess effects of our perturbations on Wnt target gene expression, we counted the number of rows of En-expressing cells in stage 9 embryos. High-level expression of Axin (Mat>Axin x Axin) significantly reduced En expression (Figure 8, K and N; average 1 row of En-expressing cells per segment, $p = 0.0004$; Schaefer *et al.*, 2018). While neither low-level zygotic expression of Axin alone (Mat>RFP x Axin; Figure 8, J and N) nor maternal and zygotic expression of Dsh alone (MatDsh x Dsh; Figure 8, L and N) had a substantial effect on *en* expression, when we combined maternal expression of Dsh with zygotic expression of Axin (Mat>Dsh x Axin), significantly fewer cells expressed *en* (Figure 8, M and N; $p < 0.0001$), mimicking the effect of high-level Axin expression (Mat>Axin x Axin; Figure 8, K and M). Thus, whether assessed by embryonic viability, cell fate choice, Arm levels, or the expression of a Wnt target gene, elevating Dsh levels can potentiate the ability of Axin to inhibit Wnt signaling.

Elevating Dsh levels in the embryo triggers Dsh assembly into cytoplasmic puncta

In stage 9 *Drosophila* embryos, endogenous Dsh accumulates in the cytoplasm of all cells and is somewhat cortically enriched in cells receiving Wnt signals (Figure 9A, red arrows; Schaefer *et al.*, 2018). Intriguingly, when we previously examined whether endogenous Dsh and Axin:GFP colocalize in puncta, we found overlap in localization in membrane-associated puncta in Wnt-ON cells (Figure 9B, yellow arrows), but no strong overlap in active destruction complex puncta in Wnt-OFF cells (Figure 9B, blue arrows; Schaefer *et al.*, 2018). Later on during dorsal closure, Dsh cortical enrichment increases in all cells and Dsh becomes planar polarized to anterior–posterior cell borders in the epidermis (Price *et al.*, 2006). To further explore the effects of Dsh and Dsh/Axin overexpression, we first examined localization of tagged Dsh constructs after overexpression. We looked at two different lines in which fluorescent–protein-tagged Dsh constructs were driven by the endogenous *dsh* promotor in a wild-type background. Dsh::GFP2.35 and Dsh::Clover are expressed at levels within a fewfold of endogenous Dsh (Schaefer *et al.*, 2018) and Dsh:GFP2.35 is a derivative of a line that rescues the *dsh* null mutant (Axelrod, 2001). In both cases, Dsh accumulated in cytoplasmic puncta in all cells at stage 9 (Figure 9, C and D), with some potential reduction in puncta number in Wnt-ON cells (Figure 9C, red arrows). Similarly, in Mat>Dsh x Dsh embryos, Dsh:Myc accumulated in apical puncta in all cells at stage 9 (Figure 9E), without obvious modulation in levels and localization with respect to cells expressing Wg. Together these data suggest that accumulation in puncta is not solely a property induced by the Myc-tag. The fact that expression of these constructs does not substantially alter Wnt signaling suggests that the puncta do not sequester Axin, consistent with the idea that Dsh needs to be "activated" to interact with Axin. This is particularly intriguing given evidence that Dsh phosphorylation may affect its ability to homopolymerize (Bernatik *et al.*, 2011; Gonzalez-Sancho *et al.*, 2013). Intriguingly, this punctate localization of the fluorescent protein-tagged Dsh proteins was stage-specific, as after dorsal closure the proteins encoded by Dsh::GFP2.35 and Dsh::Clover accumulated at the cortex in a planar-polarized manner (Figure 9, F and G), paralleling endogenous Dsh (Price *et al.*, 2006). While we must be cautious in our interpretation, due to possible overexpression artifacts, these data suggest that Dsh can form puncta, as it has been observed to do in other in vitro and in vivo settings (Yang-Snyder *et al.*, 1996; Miller *et al.*, 1999; Schwarz-Romond *et al.*, 2005), and puncta formation/size may depend on expression levels. One speculative possibility is that these puncta may also recruit endogenous Dsh, preventing it from assembling with and thus helping inactivate destruction complexes in Wnt ON-cells, providing one way by which Dsh overexpression could paradoxically inhibit Wnt signaling.

Elevating Dsh levels in the embryo does not lead to Axin recruitment into Dsh puncta

We next examined whether altering Dsh levels affects Axin localization. When expressed at levels within a fewfold of endogenous, Axin:GFP accumulates in a segmentally varying pattern of localization, with larger cytoplasmic puncta in Wnt-OFF cells (Figure 9B, blue arrows) and smaller membrane-associated puncta in Wnt-ON cells (Figure 9B, yellow arrows; Schaefer *et al.*, 2018). Axin's membrane relocalization in Wnt-ON cells requires Dsh (Cliffe *et al.*, 2003). Strikingly, Axin's segmentally varying pattern was not obviously altered after elevating Dsh levels—Axin:GFP continued to accumulate in large cytoplasmic puncta in Wnt-OFF cells and in smaller membrane-associated puncta and in the cytoplasm of Wnt-ON cells (Figure 9H, blue vs. yellow arrows; Mat>Dsh x Axin; compare to Figure 9B). Further, the Dsh puncta that assembled after Dsh:Myc overexpression (Figure 9H, magenta arrows) did not colocalize with the strong Axin puncta in either Wnt-ON or WNT-OFF cells (Figure 9H, yellow and blue arrows). These data are consistent with the idea that if Dsh is not "activated" by Wnt signaling, it cannot sequester Axin.

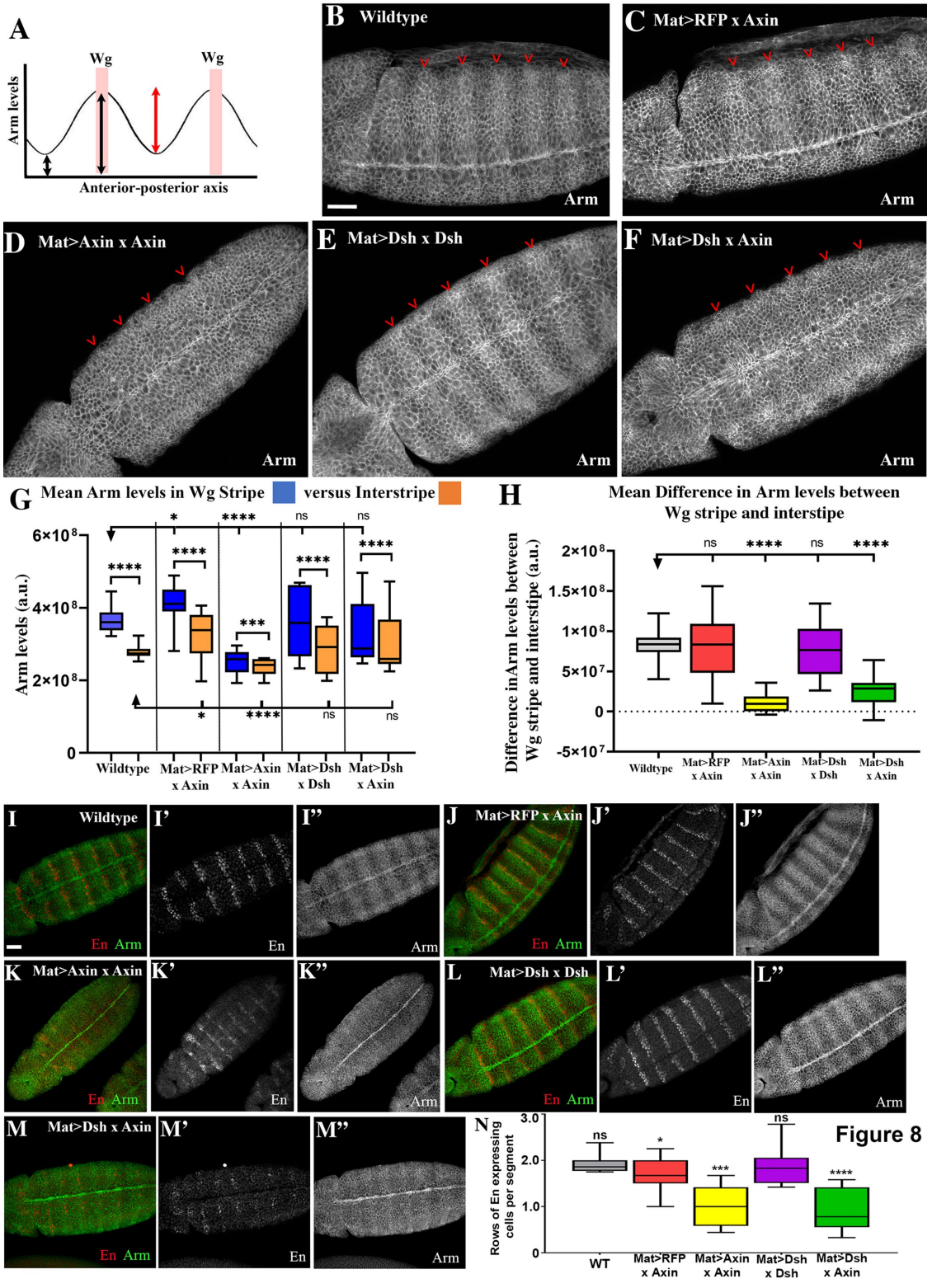

FIGURE 8: Elevating Dsh levels enhances the ability of Axin to promote Arm destruction and down-regulate the Wnt-target gene En. (A) Diagram illustrating how Wg-signaling affects Arm accumulation. Two body segments are illustrated. Within each segment a single row of cells expresses the Wnt ligand Wg (red bands), and it forms a graded distribution across the segment, stabilizing cytoplasmic/nuclear Arm in cells that receive it (derived from Schaefer *et al.*, 2018). The closer to the cells secreting Wg, the higher the accumulation of Arm in the cytoplasm and nucleus. (B–F) Arm accumulation in Stage 9 embryos, anterior to the left, of the genotypes indicated. Red arrowheads label the rows of Wg-expressing cells. (B) In wild type, Wg stabilizes Arm in a graded manner with highest levels in the cells that express Wg (quantified in G), and thus there is a large difference in levels between Arm stripes and interstripes (H). (C) Low-level zygotic expression of Axin does not substantially alter Arm stabilization by Wg signaling. (D) High-level maternal and

Finally, we examined the effect of elevating either Axin or Dsh levels on localization of APC2. Here, an effect was more apparent. In wild-type embryos, APC2 is cortically enriched in all cells (Figure 9I; McCartney *et al.*, 1999). Elevating levels of Dsh in Mat>Dsh x Dsh embryos did not alter this localization pattern (Figure 9J). Elevating Axin expression led to recruitment of cortical APC2 to Axin puncta in Wnt-OFF cells (Figure 9K, blue arrows), while cortical enrichment of APC2 in Wnt-ON cells remained (Figure 9K, red arrows; Schaefer *et al.*, 2018). Combining elevating Dsh levels with elevating Axin in Mat>Dsh x Axin embryos appeared to enhance the localization of APC2 to the plasma membrane of Wnt-ON cells (Figure 9L, yellow arrows), without altering APC localization of Axin puncta in Wnt-OFF cells (Figure 9L, blue arrows). Thus elevating Dsh levels may enhance the effects of Axin overexpression on APC2 localization. One speculative possibility is that this could occur because all of the Dsh is assembled into ectopic puncta, thus preventing it from competing with APC2 for access to Axin. This might increase localization of APC2 with Axin near the Wnt receptors in Wnt-ON cells, where Dsh might otherwise displace it, reducing inactivation of the destruction complex. We discuss this and other possibilities in the *Discussion*.

SIM imaging suggests relative levels of Axin and Dsh may alter their interactions

Our earlier work and that of others illustrated the ability of SIM to begin to define the internal structure of the destruction complex, revealing intertwined polymers of Axin and APC or of Axin and Tankyrase when these proteins are expressed in cultured human cells (Pronobis *et al.*, 2015; Thorvaldsen *et al.*, 2015). Like Axin, Dsh forms puncta when expressed in cultured cells. We took a similar approach to better understand the structure of Dsh puncta utilizing SIM. We tagged Dsh at the N-terminus or the C-terminus with either GFP or RFP and transfected these constructs into SW480 cells. When expressed alone, Dsh forms puncta when tagged with fluorescent proteins either at the N- or at the C-termini (Figure 10, A and B)—thus tag localization does not affect the ability of the N-terminal DIX domain to self-polymerize and help drive puncta formation (Schwarz-Romond *et al.*, 2005, 2007a,b; Fiedler *et al.*, 2011). Dsh expression had no apparent effect on levels or localization of βcat. Dsh formed two different categories of puncta in different cells: smaller, more spherical puncta (Figure 10, A and B) or larger, more complex puncta (Figure 10, C and D), potentially due to the level of Dsh expression. We then used SIM to look inside the more complex puncta to see if the Dsh formed an underlying structure within them. When expressed alone, Dsh:RFP in puncta resolved into a loose network of intertwined filaments, potentially representing DIX domain-mediated polymers, (Figure 10D), similar to but more complex than the polymers formed by Axin:RFP expressed alone (Figure 11, A and B; Pronobis *et al.*, 2015). When coexpressed, Dsh:GFP and RFP:Dsh largely coassembled into these filaments (Figure 10, E and E1), suggesting these are not a property of the tag or its location and consistent with the idea that they copolymerize. The complexity of the Dsh polymers resembled the complexity of the intertwined Axin and APC2 cables formed after coexpression (Figure 6, H, H1, and I; Pronobis *et al.*, 2015).

Previous work provided evidence that Dsh and APC compete for access to Axin, and that the Dsh association with Axin inhibits destruction complex function (Cliffe *et al.*, 2003; Schwarz-Romond *et al.*, 2005; Mendoza-Topaz *et al.*, 2011). Both Dsh and Axin can homopolymerize via their DIX domains and can also heteropolymerize (Schwarz-Romond *et al.*, 2005, 2007a,b; Fiedler *et al.*, 2011). Our SW480/SIM system provided an opportunity to explore the Dsh:Axin interaction in vivo at superresolution. Previous studies revealed that Axin and Dsh can colocalize in cytoplasmic puncta when coexpressed in cells (Fagotto *et al.*, 1999; Kishida *et al.*, 1999; Julius *et al.*, 2000; Fiedler *et al.*, 2011). We thus used SIM to examine puncta formed after coexpression of fluorescently tagged Axin and

zygotic expression of Axin largely abolishes Wg stabilization of Arm. (E) High-level maternal and zygotic expression of Dsh does not abolish the graded pattern of Arm accumulation. (F) Combining high-level maternal and zygotic expression of Dsh with low-level zygotic expression of Axin substantially reduces the ability of Wg to stabilize Arm. (G) Quantification of mean total Arm levels in two cell rows with high Wg signaling (Wg stripe) vs. two rows of cells farthest from Wg expressing cells (Interstripe). Box and whisker plots. Boxes cover 25th–75th percentiles and whiskers the minimum and maximum. Median = middle line; $n = 8$ embryos per genotype. A paired *t* test was used to compare intragroup Arm levels (stripe vs. interstripe within the same embryo). An unpaired *t* test was used to compare Arm levels in either the stripe or the interstripe between genotypes since Arm levels are independent between groups. Probability that stripe and interstripe values are the same within a genotype: wild type $p < 0.0001$; Mat>RFP x Axin $p < 0.0001$; Mat>Axin x Axin $p = 0.0002$; Mat>Dsh x Dsh $p < 0.0001$; Mat>Dsh x Axin $p < 0.0001$. Probability that levels of Arm in the stripe are the same from those in the wild-type stripe: Mat>RFP x Axin $p = 0.181$; Mat>Axin x Axin $p < 0.0001$; Mat>Dsh x Dsh $p = 0.810$; Mat>Dsh x Axin $p = 0.0725$. Probability that levels of Arm in the interstripe are the same as those in the wild-type interstripe: Mat>RFP x Axin $p = 0.0294$; Mat>Axin x Axin $p < 0.0001$; Mat>Dsh x Dsh $p = 0.9695$; Mat>Dsh x Axin $p = 0.3276$. (H) Plot of the difference between Arm levels in the Wg stripe vs. interstripe per embryo. Boxes and whiskers as in G; $n = 3$ stripes from each of 8 embryos. An unpaired *t* test was used to compare the difference of Arm levels of the Stripe and Interstripe between genotypes. Probability that the difference in Arm levels in the stripe vs. interstripe is the same as that in wild type: Mat>RFP x Axin $p = 0.9468$; Mat>Axin x Axin $p < 0.0001$; Mat>Dsh x Dsh $p = 0.5169$; Mat>Dsh x Axin $p < 0.0001$. (I–M) Representative images of Stage 9 embryos of the genotypes indicated, stained for En and Arm. Anterior is to the left. (I) In wild type, the two posterior rows of cells in each genotype express En. (J) Low-level zygotic expression of Axin does not substantially alter the number of cells expressing En. (K) High-level maternal and zygotic expression of Axin reduces the number of cells expressing En. (L) High-level maternal and zygotic expression of Dsh does not substantially alter the number of cells expressing En. (M) Combining high-level maternal and zygotic expression of Dsh with low-level zygotic expression of Axin substantially reduces the number of En-expressing cells. (N) Quantification of the number of rows of En-expressing cells per segment; $n = 8$ embryos for wild type and 9 for all other genotypes. Boxes and whiskers as in G. A one sample *t* test was used to analyze the number of rows of En cells per segment, since the known value of En cells per segment in wild type is 2. Probability that the number of rows of En-expressing cells is not different than 2: Wild type $p = 0.36$; Mat>RFP x Axin $p = 0.04$; Mat>Axin x Axin $p = 0.0004$; Mat>Dsh x Dsh $p = 0.41$; Mat>Dsh x Axin $p < 0.0001$. Scale bars = 30 μm. In all graphs, ns = nonsignificant; *<0.05; **<0.005; ***<0.0005, ****<0.0001.

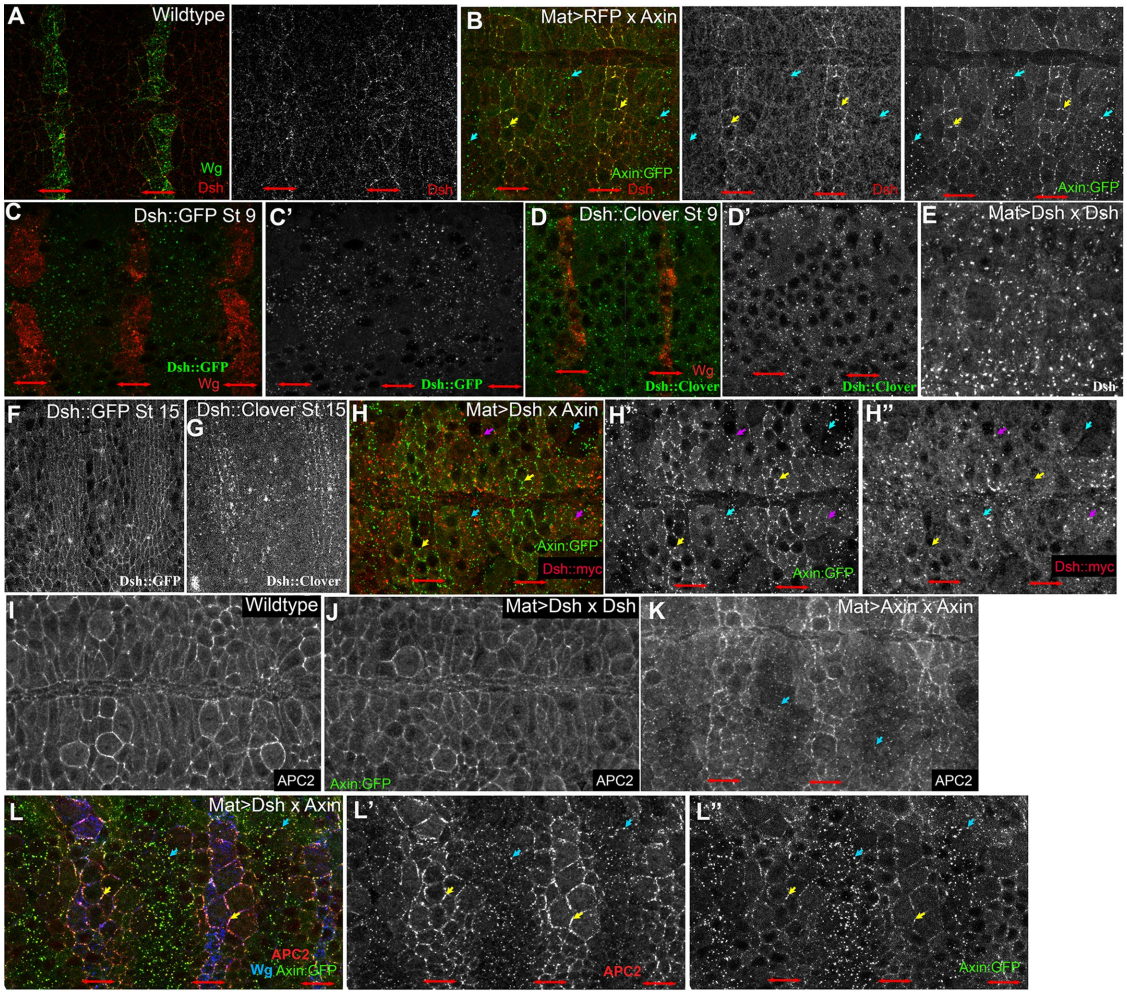

FIGURE 9: When Dsh expression levels are elevated, it forms cytoplasmic puncta but they do not colocalize with Axin. Embryos, anterior to the left, genotypes, and antigens indicated. All are stage 9 except F and G, which are stage 15. (A) At stage 9 endogenous Dsh is cytoplasmic in all cells with weak membrane enrichment in Wnt-ON cells (in this and subsequent panels, WNT-ON cells are indicated by red double-headed arrows). (B) Low-level overexpression of Axin (Mat>RFP x Axin) enhances recruitment of endogenous Dsh to the membrane of Wnt-ON cells, where it colocalizes with Axin (yellow arrows), but Dsh is not recruited to the cytoplasmic Axin puncta in Wnt-OFF cells (blue arrows). (C–D) Two different fluorescent protein tagged Dsh proteins driven by the endogenous *dsh* promotor both form cytoplasmic puncta at stage 9. (E) In Mat>Dsh x Dsh embryos, Dsh:myc forms prominent apical cytoplasmic puncta in all cells. (F, G) Two different fluorescent protein tagged Dsh proteins each relocalize to the cortex in a planar-polarized manner at stage 15, thus resembling endogenous Dsh (Price *et al.*, 2006). (H) In Mat>Dsh x Axin embryos (high-level Dsh, low Axin), the normal alternating pattern of membrane-associated Axin puncta in Wnt-ON cells (yellow arrows) and cytoplasmic Axin puncta in Wnt-OFF cells (blue arrows) is unchanged. Dsh:myc forms cytoplasmic puncta (magenta arrows) but these do not strongly recruit Axin. (I) In wild-type embryos, APC2 is enriched at the cortex of all cells. (J) In Mat>Dsh x Dsh embryos, APC2 localization is unchanged. (K) Elevating Axin expression (Mat>Axin x Axin) leads to preferential accumulation of APC2 at the cortex of Wnt-ON cells (red arrows) and coaccumulation with Axin in cytoplasmic puncta in Wnt-OFF cells (blue arrows). (L) In Mat>Dsh x Axin embryos (high-level Dsh, low Axin), the recruitment of APC2 to the cortex of Wnt-ON cells is enhanced (yellow arrows). Scale bar = 15 μm.

Dsh. When expressed alone, Axin puncta contain tightly curved Axin polymers (Figure 11, A and B; Pronobis *et al.*, 2015). Interestingly when we coexpressed Dsh and Axin, we found that Axin–Dsh puncta interactions varied across a spectrum, with variation primarily between cells rather than within cells. In some cells, seemingly those with relatively low levels of Dsh expression, strong overlap in localization, with partial "colocalization" of Dsh and Axin, was revealed when puncta were observed at superresolution (Figure 11, C and D; 37/169 cells examined; Table 3A). Puncta in this subset of cells formed donut or pretzel shapes (Figure 11, C1, C2, and D), similar to those seen when Axin is expressed alone (Figure 11, A1 and B). However, in cells that appeared to have higher levels of Dsh expression, Axin–Dsh puncta interactions were altered. In a subset of these cells, Dsh continued to overlap/colocalize with Axin, but these puncta also had adjacent Dsh structures containing lower levels of Axin or no Axin (Figure 11, E, E1, and E2; 42 of 169 cells observed; Table 3A). Finally, in about half of the cells, Dsh and Axin puncta segregated (Figure 11, F–I; 90/169 cells observed; Table 3A). In this category of cells Axin puncta substructure remained largely unchanged, with primarily small, donut-shaped puncta (Figure 11, F1, F2, G, and H1). However, Dsh puncta were larger and more complex (Figure 11, F1, G, and H1), resembling what we saw in cells

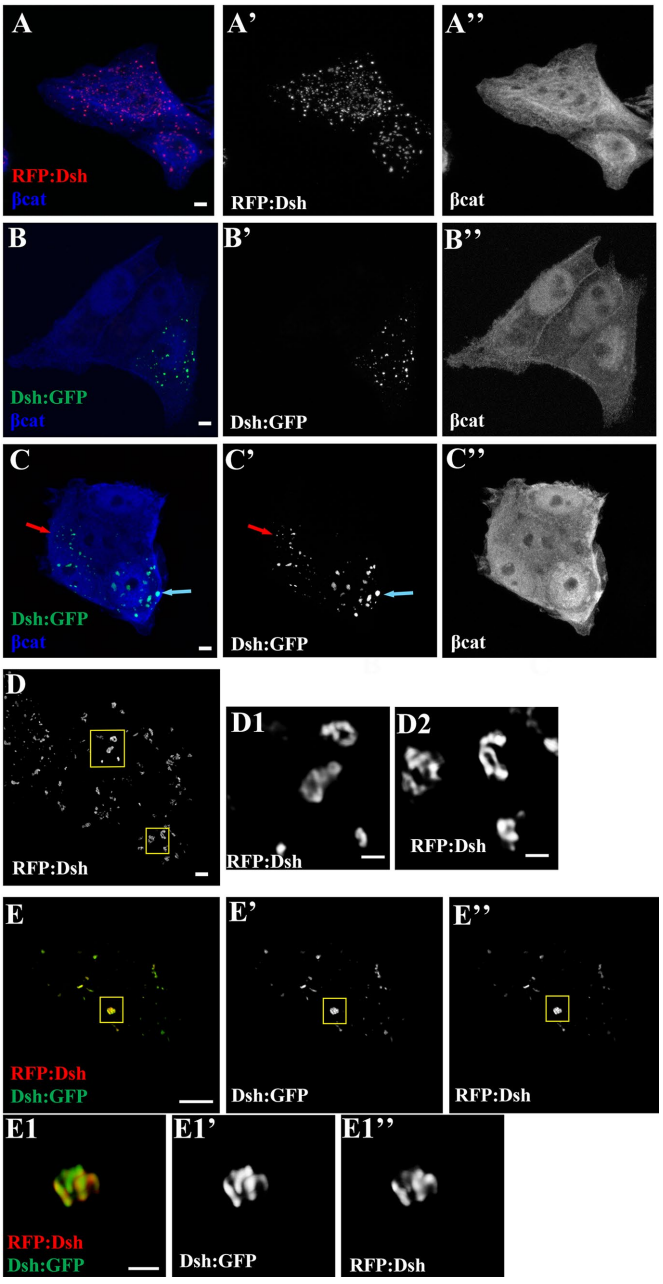

FIGURE 10: SIM imaging reveals structure inside Dsh puncta. SW480 colorectal cancer cells transfected with the indicated constructs, with fluorescence of the tagged protein imaged directly. (A–E) Whole cells. Scale bars = 10 μm. (D1, D2, E1) Close-ups of puncta. Scale bars = 0.5 μm (A, B) Confocal images of cells transfected with an N-terminal RFP-tagged Dsh (A) or a C-terminal GFP-tagged Dsh (B), stained for βcat. Both constructs form similar-looking puncta, suggesting that tag location has little effect on puncta formation. (C) Representative image of two cells, expressing lower (red arrow) or higher (blue arrow) levels of Dsh. In cells expressing higher levels of Dsh, puncta are larger and less spherical. (D, D1, D2) SIM image of a cell expressing RFP-Dsh, with close-ups of several larger puncta (indicated by boxes). SIM close-ups reveal that many puncta have a complex internal structure of polymers. (E, E1) SIM image of a cell coexpressing RFP:Dsh and Dsh:GFP. In close-ups of puncta, there is intermixing and some colocalization of both versions of tagged Dsh in the tangled polymers.

expressing higher levels of Dsh alone (Figure 10, D1 and E1). Rather than colocalizing or strongly overlapping with Axin in puncta, we observed complex Dsh structures surrounding (Figure 11, F1 and H1) or docked on (Figure 11G) donut-shaped Axin puncta. In many of these cells, there was little or no colocalization. To further explore the idea that relative levels of Dsh/Axin might be a factor, we varied the ratios of Axin:Dsh DNA used in transfection—while this does not eliminate cell–cell variability, we scored multiple cells that were representative of what we observed on each slide. Consistent with the ratio idea, when Axin:Dsh DNA levels were relatively high, fewer cells had segregation and more had colocalization (Table 3B); however, this should be independently verified in the future by more direct measurements of relative protein levels. Together these data suggest the speculative possibility that altering relative levels of Axin and Dsh might affect homo-oligomerization versus hetero-oligomerization by an as yet unknown mechanism. In vivo, this could provide a potential regulatory mechanism.

DISCUSSION

Wnt signaling plays key roles in development and disease by regulating the stability of its effector βcat. In the absence of Wnt signals, βcat is phosphorylated by the Wnt-regulatory destruction complex, ubiquitinated by an SCF-class E3 ubiquitin ligase, and destroyed by the proteasome. Binding of Wnt ligands to their Frizzled/LRP receptors stabilizes βcat via the cytoplasmic effector Dsh. Here we explore two important questions in the field: Is there a direct transfer of βcat from the destruction complex to the E3 ligase, and how does Dsh interaction with the destruction complex protein Axin regulate destruction complex function?

Defining mechanisms by which βcat is transferred from the destruction complex to the E3 ubiquitin ligase

Regulating the stability of βcat is the key step in Wnt signaling (Peifer *et al.*, 1994; van Leeuwen *et al.*, 1994). The SCF^{Slimb} E3 ligase was first identified as the relevant E3 regulating βcat levels in 1998 (Jiang and Struhl, 1998; Marikawa and Elinson, 1998). It specifically recognizes βcat after its sequential phosphorylation by CK1 and GSK3 (Hart *et al.*, 1999; Kitagawa *et al.*, 1999; Liu *et al.*, 1999), and the most N-terminal phosphoserine is a key part of the binding site for the F-box protein Slimb/βTrCP (Orford *et al.*, 1997; Wu *et al.*, 2003). Phosphatase activity in the cytoplasm can rapidly dephosphorylate this residue, raising the question of how βcat is transferred to the E3 ligase without being dephosphorylated. Earlier work offered two clues. First, βTrCP can co-IP with Axin and APC (Hart *et al.*, 1999; Kitagawa *et al.*, 1999; Liu *et al.*, 1999; Li *et al.*, 2012), suggesting it may associate, at least transiently, with the destruction complex, providing a potential transfer mechanism. Consistent with this, stabilizing Axin using Tankyrase inhibitors led to colocalization of βTrCP and Tankyrase with the destruction complexes that assemble in response (Thorvaldsen *et al.*, 2015). However, it was not clear if this occurred by a direct interaction of βTrCP with destruction complex components via bridging by phosphorylated βcat or occurred because other components of the SCF^{Slimb} E3 ligase were recruited more directly, with βTrCP recruited as a secondary consequence. A second clue emerged from analyses revealing that one role for APC is to prevent dephosphorylation of βcat while it is in the destruction complex, protecting the βTrCP binding site (Su *et al.*, 2008).

Two plausible models were suggested by these data. In the first, the entire SCF^{Slimb} E3 ligase might be recruited to the destruction complex, allowing direct transfer of phosphorylated βcat between

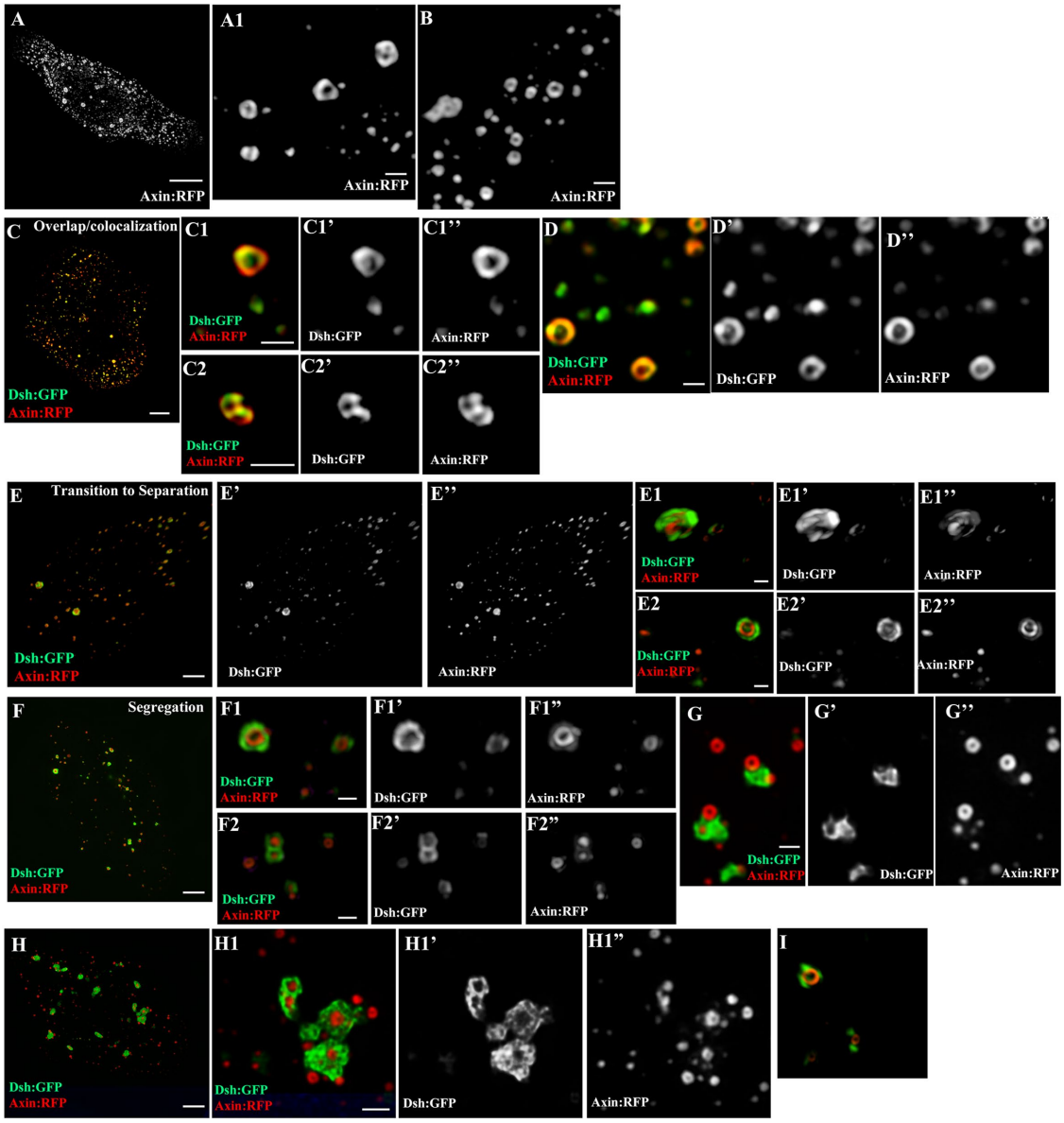

FIGURE 11: Dsh and Axin can either colocalize in puncta or segregate. SIM imaging of SW480 colorectal cancer cells transfected with the indicated constructs, with fluorescence of the tagged protein imaged directly. (A, C, E, F, H) Whole cells. (A1, B, C1, C2, D, E1, E2, F1, F2, G, H1, I) Close-ups of puncta. (A, B) When Axin is expressed alone, most Axin puncta contain tight circular Axin polymers. (C–I) Cells expressing both Dsh:GFP and Axin:RFP. (C, D) Representative images from cells with low-level Dsh expression. (C1, C2, D) Close-up images of puncta from C or a similar cell, revealing strong overlap or colocalization of Axin and Dsh. (E) Representative image of a cell in which Axin and Dsh appear to transition into more complete separation. (E1, E2) Close-up of puncta from E. Axin:RFP is more enriched in the center of the punctum, while Dsh:GFP is more enriched in the outer region. (F, H) SIM image of cells with higher level Dsh expression, in which Dsh puncta are larger and Dsh/Axin segregation is more prominent. (F1, F2, G, H1, I) Close-ups of punctum from F and H and similar cells. Dsh puncta were larger and more complex, while Axin continued to form small circular polymers. Rather than colocalizing or strongly overlapping with Axin in puncta, Dsh puncta surrounded (F1, F2, G, H1) or docked on (G, H1, I) Axin puncta. Scale bars = 3 μm for whole cell images and 0.5 μm for close-ups. Similar letter labels indicate close-ups from the same cell (e.g., H and H1), while different letter labels are close-ups from additional cells with similar degrees of segregation (e.g., H and I).

the two complexes. In a second model, βTrCP could serve as a shuttle, binding to phosphorylated βcat at the destruction complex and shuttling it to a place where the E3 assembled and ubiquitinated βcat.

We explored interactions of the E3 ligase with the destruction complex using cell biological assays in SW480 cells. We observed ready recruitment of the βTrCP homologue Slimb to destruction complex puncta by Axin, but did not observe recruitment by APC2, consistent with earlier assays by co-IP (Kitagawa *et al.*, 1999). Slimb recruitment did not require the βcat-binding site of Axin, making it less likely that recruitment occurs solely via bridging by βcat. However, it was enhanced by the RGS domain of Axin—future work to assess whether this involves a direct interaction or whether an indirect one is warranted. There are conserved residues in the RGS

(A) Summary of the different types of interactions between Axin and Dsh					
Protein combination	**Strong overlap in localization**	**Transition to separation**	**Segregation**	**Total number of cells analyzed**	**Number of experiments**
Axin + Dsh	37	42	90	169	13

(B) Axin to Dsh transfection ratio may affect the degree of protein–protein colocalization					
Axin:Dsh protein ratio	**Strong overlap in localization**	**Transition to separation**	**Segregation**	**Total number of cells analyzed**	**Number of experiments**
1 to 4			3	3	1
1 to 2		2	12	14	3
1 to 1		5	12	17	3
2 to 1	1	6	10	17	2
3 to 1	3	2	2	7	1
4 to 1	1	3	9	13	1
6 to 1	5	1	0	6	1

TABLE 3: (A) Summary of the different types of interactions between Axin and Dsh, including number of cells imaged. Strong overlap in localization, puncta are simple in shape and Axin and Dsh substantially overlap, resulting in yellow puncta. Transition to Separation, Axin and Dsh still exhibit substantial overlap but there are also regions of distinct localization. Segregation, Axin and Dsh proteins no longer appear to overlap although they often dock next to one another. Number of experiments equals the number of independent times cells were transfected with the labeled protein combinations. (B) Degree of colocalization observed at different Axin to Dsh transfection ratios. Ratios reflect Axin and Dsh plasmid concentrations used for transfections. The higher the Axin:Dsh ratio, the more complete the colocalization.

domain that are not necessary for the APC–Axin interaction, some of which form a pi helix, and it will be interesting to further explore the function of these residues (Spink *et al.*, 2000). Both the region containing the N-terminus plus the F-box of Slimb and that including its WD40 repeats could be separately recruited into Axin puncta, suggesting it may be recruited by multiple interactions—in the case of the WD40 repeats, this could include bridging by phosphorylated βcat. Once again, direct binding assays in vitro would provide further insights, building on earlier assays suggesting a multipartite binding interaction (Kitagawa *et al.*, 1999). Our super-resolution imaging suggests the interaction between Slimb and Axin is intimate, consistent with direct binding. Our FRAP data, on the other hand, reveal that Slimb can come in and out of the complex, similar to the behavior of Axin and APC.

In contrast to the strong recruitment of Slimb to destruction complex puncta, two other core components of the SCF^{Slimb} E3 ligase, Skp1 and Cul1, were not avidly recruited. The occasional recruitment seen could reflect interactions with endogenous βTrCP in the puncta. Coexpression of SkpA or Cul1 with Slimb slightly enhanced recruitment, but this was still not as robust as the recruitment of Slimb itself. Our IP/mass spectroscopy data and earlier work from the Mann lab (Hilger and Mann, 2012) are consistent with the presence of all three core SCF^{Slimb} E3 ligase proteins in the destruction complex, but suggest they may be present at lower levels than core destruction complex proteins. One possibility is that Slimb/βTrCP usually acts as a shuttle, but its presence occasionally recruits the other E3 proteins. Another possibility is that the entire SCF^{Slimb} E3 ligase docks on the destruction complex transiently to accept phosphorylated βcat, ubiquitinate it, and then transfer it to the proteasome. Consistent with this possibility, inhibiting Tankyrase not only stimulates association of βTrCP with Axin but also leads to recruitment of the proteasome itself to the destruction complex (Thorvaldsen *et al.*, 2015)—intriguingly, proteasome inhibition reduces destruction complex assembly, though this effect appears to be indirect due to effects on Axin2 levels (Pedersen *et al.*, 2016). Further analyses will be needed to discriminate between these possibilities.

Additional work is also needed to explore how βcat transfer to the E3 ligase is regulated. Direct targeting of βcat to the E3, by fusing the F-box of Slimb with the βcat-binding sites of Tcf4 and E-cadherin, is sufficient to stimulate βcat destruction, independent of the destruction complex (Liu *et al.*, 2004), but in vivo the destruction complex plays a critical role. Several pieces of data are consistent with the idea that transfer of βcat to the E3 ligase is the step regulated by Wnt signaling, rather than phosphorylation of βcat, with APC having an important role (Li *et al.*, 2012; Pronobis *et al.*, 2015). Further exploration of this process will be welcome.

Dsh and Axin: a complex interaction

It has been clear for more than two decades that Dsh is a key effector of Wnt signaling (Klingensmith *et al.*, 1994; Noordermeer *et al.*, 1994). However, its precise mechanisms of action are complex and not fully understood. Current data suggest that Dsh is recruited to activated Frizzled receptors via its DEP domain (Tauriello *et al.*, 2012; Gammons *et al.*, 2016b). Dsh then helps ensure the Wnt-dependent phosphorylation of LRP5/6 (Bilic *et al.*, 2007; Metcalfe *et al.*, 2010), leading to receptor clustering, facilitating Axin recruitment, and thus inhibiting GSK3 (Tamai *et al.*, 2004; Stamos *et al.*, 2014). Dsh homo-polymerization, via its DIX domain, and hetero-polymerization with Axin (Fiedler *et al.*, 2011), along with DEP-domain dependent Dsh cross-linking (Gammons *et al.*, 2016a), are then thought to lead to down-regulation of the destruction complex and thus stabilization of βcat.

Intriguingly, in *Drosophila* embryos Dsh, Axin, and APC are present at levels within a fewfold of one another (Schaefer *et al.*, 2018). Many current models suggest that relative ratios of these three proteins are critical to the signaling outcome, with APC and Dsh competing to activate or inhibit Axin, respectively. Consistent with this, substantially elevating Axin levels in vivo, using *Drosophila* embryos as a model, renders the destruction complex immune to down-regulation by Wnt signaling (Willert *et al.*, 1999; Cliffe *et al.*, 2003). Subsequent work revealed that the precise levels of Axin are critical—elevating Axin levels by two- to fourfold has little effect, while elevation

by ninefold is sufficient to constitutively inactivate Wnt signaling (Wehrli *et al*., 2000; Wang *et al*., 2016; Schaefer *et al*., 2018). One might then predict that elevating Dsh levels would have the opposite effect, sequestering Axin and thus stabilizing βcat and activating Wnt signaling. While very high levels of Dsh overexpression can have this effect (Wehrli *et al*., 2000; Cliffe *et al*., 2003), we previously were surprised to learn that sevenfold elevation of Dsh levels only had a subtle effect on Wnt signaling and thus had little effect on embryonic viability (Schaefer *et al*., 2018). Our data further suggested that Dsh is only recruited into Axin puncta in cells that received Wg signal, in which puncta are recruited to the plasma membrane, even though seemingly similar levels of Dsh were present in Wnt-OFF cells (Schaefer *et al*., 2018). This opened the possibility that a Wnt-stimulated activation event, such as Dsh phosphorylation (e.g., Yanagawa *et al*., 1995; Gonzalez-Sancho *et al*., 2004), might be required to facilitate Dsh interaction with Axin and thus Axin inactivation. In this scenario, elevating Dsh levels in cells without this activation event, for example, in Wnt-OFF cells, would not alter signaling output.

The simplest versions of the antagonism model, involving competition between formation of Axin/APC versus Axin/Dsh complexes, would also suggest that elevating Dsh levels should alleviate effects of elevating Axin. Here we tested this directly, expressing high levels of Dsh maternally and lower levels of Axin zygotically. We anticipated that elevating Dsh levels would blunt the effects of elevating levels of Axin. Instead, we got a substantial surprise: elevating levels of Dsh enhanced the ability of Axin to resist turndown by Wnt signaling, thus leading to global activation of the destruction complex and inactivation of Wnt signaling. This was true whether we assessed effects on cell fate choice, Arm levels, or expression of a Wnt-target gene. Intriguingly, our data were also consistent with the possibility that elevating Dsh levels may alter Axin:APC interactions in Wnt-ON cells—this might provide a clue to an underlying mechanism.

What could explain this paradoxical result? Our current data do not provide a definitive answer but do open some intriguing possibilities and new questions. In our view, part of the explanation will be that Wg-dependent "activation" of Dsh is required for it to interact with and thus down-regulate Axin. Consistent with this, Dsh phosphorylation can regulate its ability to homopolymerize (Bernatik *et al*., 2011; Gonzalez-Sancho *et al*., 2013). By elevating Dsh levels, we may have exceeded the capacity of this activation system. High levels of "nonactivated" Dsh, while unable to interact with Axin, might still interact with other key proteins involved in destruction complex down-regulation, sequestering them in nonproductive complexes. For example, Dsh can bind CK1 (Peters *et al*., 1999; Sakanaka *et al*., 1999; Kishida *et al*., 2001), which has complex roles in Wnt regulation (Harnoš *et al*., 2018). With key proteins sequestered, the system might become less able to inactivate the slightly elevated levels of Axin present, thus leading to constitutive activity of the destruction complex. In this speculative scenario, it is not the relative levels of Axin and Dsh that are key but the relative levels of Axin and "active Dsh."

The results of our SIM experiments may also provide insights. The ability of Axin and Dsh to both homo- and hetero-polymerize means free monomers must make a choice. It is likely this is a regulated choice, though the mechanism of regulation remains unclear. Our SW480 experiments, while overly simple, may provide an illustration of how the homo-/hetero-polymerization balance can shift. In cells in which both Axin and Dsh were expressed at relatively low levels, puncta contained both proteins, and internal structure was consistent with some level of hetero-polymerization. In contrast, when levels of Dsh were significantly higher, Axin and Dsh tended to segregate into separate, adjoining puncta, suggesting the balance was shifted to homo-polymerization, though the polymers retained the ability to dock on one another. If similar events occur on elevating Dsh expression in *Drosophila* embryos, segregation could allow Axin to remain in functional destruction complexes, even in Wnt-ON cells, while Dsh localized to separate puncta sequestered other Wnt-regulating proteins, potentially explaining how elevating Dsh expression could paradoxically down-regulate Wnt signaling. Elevating Dsh levels may also lead it to preferentially associate with itself, as was suggested by our SIM data in SW480 cells—this could recruit endogenous Dsh away from its normal localization with the destruction complex, thus preventing it from participating in inactivating Axin. Defining the mechanisms that determine the relevant affinities of each protein for itself versus for its partner will be informative. Intriguingly, we observed a similar docking rather than coassembly behavior when we imaged the puncta formed by Axin and those formed by the Arm repeat domain of APC2 (Pronobis *et al*., 2015)—this may be another example where relative affinities of proteins for themselves versus their binding partners differ.

Very recent work provides important new insights in this regard. Yamanishi *et al*. (2019) determined the structure of the heterodimer of the DIX domains of Dsh and Axin and also measured their relative affinities for one another. Kan *et al*., (2020: Preprint) used cryo-electron microscopy to solve the structure of Dsh filaments and also measured affinities of DIX domains of Dsh and Axin. Their results contrast, with the first group suggesting Dsh homodimerization is an order of magnitude more favorable than Axin homodimerization, while heterodimerization is intermediate in affinity, and the other suggesting Axin homodimerization is most favorable. Resolution of this will be important, as we assess how Dsh acts to turn down destruction complex activity by heterodimerization. It also is interesting given our in vivo observations that APC may help stabilize Axin homo-polymerization (Pronobis *et al*., 2015). These data also may help explain our results in SIM, where segregation of Dsh and Axin is favored in some circumstances. Defining the in vivo regulatory mechanisms that modulate homo- and heteropolymerization will be an important goal. Together our results leave us with more questions than answers but suggest that there are important features of Wnt signaling in vivo yet to be uncovered. Further cell biological and biochemical experiments in vivo, combined with new mathematical models of the suspected competition, will be extremely useful.

MATERIALS AND METHODS

Fly stocks, embryonic lethality, and cuticles

All fly stocks, crosses, and embryo experiments were performed at 25°C. For this study: *y w* was used as wild type. The following stocks were obtained from the Bloomington Stock Center: Maternal alpha tubulin GAL4 (referred to as MatGAL4; a stock carrying both of the GAL4 lines in 7062 and 7063), UAS-Axin:GFP (7225), UAS-Dsh:Myc (9453), and UAS-RFP (30556). Embryonic lethality assays and cuticle preparations were as in Wieschaus and Nüsslein-Volhard (Wieschaus and Nüsslein-Volhard, 1986). Inhibition and/or overexpression of Wg signaling was assessed by analyzing embryonic and first instar larvae cuticles with the scoring criteria found in Schaefer *et al*. (2018).

Cross abbreviations (Female x Male):

Mat>RFP x Axin = UAS-RFP/MatGAL4; +/MatGAL4 females x UAS-Axin:GFP males

Mat>Axin x Axin = +/MatGAL4; UAS-Axin:GFP /MatGAL4 females x UAS-Axin:GFP males

Mat>Dsh x Dsh = +/MatGAL4; UAS-Dsh:Myc/MatGAL4 females x UAS-Dsh:Myc males

Mat>Dsh x Axin = +/MatGAL4; UAS-Dsh:Myc/MatGAL4 females x UAS-Axin:GFP

Mat>Dsh x RFP = +/MatGAL4; UAS-Dsh:Myc/MatGAL4 females x UAS-RFP males

Embryo immunostaining and antibodies

Flies were allowed to lay eggs on apple juice/agar plates with yeast paste for up to 7 h. A paintbrush was then used to collect embryos in 0.1% Triton-X in water and eggs were dechorionated in 50% bleach. After fixation for 20 min in 1:1 heptane to 9% formaldehyde, with 8 mM EGTA added to preserve GFP expression, embryos were devitellinized in 1:1 heptane to methanol. Embryos were then washed in methanol followed by 0.1% Triton-X in phosphate-buffered saline (PBS), then incubated in blocking buffer (1:1000 normal goat serum [NGS] diluted in 0.1% Triton-X in PBS) for 30 min. Primary antibody incubation occurred overnight at 4°C. Embryos were washed in 0.1% Triton-X in PBS and then incubated in secondary antibody at room temperature for 1 h. Embryos were mounted in Aqua Polymount (Polyscience). Primary antibodies were: Wingless (Wg, Developmental Studies Hybridoma Bank [DSHB]:4D4, 1:1000), Arm (DSHB:N27 A1, 1:75), En (DSHB:4D9, 1:50), APC2 (McCartney *et al*., 1999; 1:1000), and Dsh (Shimada *et al*., 2001; 1:4000).

Assessing effects on En expression

To determine the transcriptional output of Wg signaling, En expression was analyzed in stage 9 embryos. En antibody-stained embryos were imaged on a Zeiss LSM 710 or 880 scanning confocal microscope. Images were processed as in Schaefer *et al.* (2018). Briefly, Fiji (Fiji Is Just ImageJ) was used to generate maximum intensity projections 8 µm thick. The En channel was then thresholded to highlight En-expressing cells. The number of rows of En-expressing cells were counted in three different locations per En stripe in thoracic/abdominal stripes 2 through 5. The number of rows of cells per En stripe was then determined by averaging these three values. Embryos were scored blind. Significance was assessed using a one-sample *t* test to analyze the number of rows of En-expressing cells per segment since the known value of rows of En cells per segment is 2 (e.g., DiNardo *et al*., 1988).

Quantitative analysis of Arm levels in Wg stripes versus interstripes

To calculate the absolute levels of Arm accumulation in cells receiving or not receiving Wg signals, stage 9 embryos were collected and stained as described above. Each genotype was imaged on the same day under the same microscope settings. To calculate the level of Arm accumulation, we chose a boxed region 100 pixels wide × 30 pixels high, spanning the width of the Wg-expressing cells, and measured the mean gray value of Arm using Fiji. Three Wg stripe regions from parasegments 2 to 4 were measured, and the average Arm value minus the background value from a region outside the embryo was defined as the Wg stripe Arm value. In the adjacent interstripe regions, we used the same box size to measure and calculate Interstripe Arm values. We also measured the relative difference in Arm accumulation between the Wg Stripes and the Interstripes. To determine the significance between intragroup values (Stripe vs. Interstripe within the same genotype), a paired *t* test was used since we were comparing Arm levels within the same embryo. An unpaired *t* test was used to determine the significance between intergroup values (e.g., Stripe vs. Stripe of different genotypes) since Arm levels were independent between groups. For multiple comparisons, an ordinary one-way ANOVA followed by Dunnett's multiple comparisons test were applied.

Cell culture and transfection

For all cell culture experiments, the human colorectal cancer cell line, SW480, was used. It was obtained from the Tissue Culture Facility at University of North Carolina's Lineberger Comprehensive Cancer Center and is ATCC line CCL228. Cells were maintained in L-15 media (Corning) supplemented with 10% heat-inactivated fetal bovine serum and 1× Pen/Strep (Life Technologies) at 37°C with ambient CO_2 levels. For transfection of *Drosophila* proteins into SW480 cells, Lipofectamine 2000 (Life Technologies) was used for transient transfection following manufacturer's instructions. All constructs contained the pCMV-backbone and Drosophila genes were inserted using the pCR8/Gateway protocol (Invitrogen) and tagged with GFP, RFP, or Flag as described in Pronobis *et al.* (2015).

Cell immunofluorescence and microscopy

Cells grown on coverslips were collected for immunofluorescence 24 h after transfection. Cells were washed in PBS and then fixed in 4% formaldehyde for 5 min. Cells were then permeabilized with 0.1% TritonX-100 in PBS for 5 min. After 30 min in block buffer (0.01% NGS in PBS), cells were incubated in primary antibody for 1–2 h, washed with PBS, and then incubated in secondary antibody for 1–2 h. Cells were mounted on microscope slides in Aqua polymount (Polyscience). Primary antibodies used: anti-βCatenin (BD Transduction, 1:800) and anti-M2-Flag (Sigma, 1:1000). Immunostained cells were imaged on an LSM Pascal microscope (Zeiss), an LSM 710 (Zeiss), or an LSM 880 (Zeiss). All images were processed using Fiji to create maximum intensity projections, and Photoshop CS6 (Adobe, San Jose, CA) was used to adjust input levels so that the signal spanned the entire output grayscale and to adjust brightness and contrast.

Super-resolution microscopy

Transiently transfected cells were stained and collected as above. Cells were mounted in Aqua polymount (Polyscience) and coverslips were sealed with nail polish to prevent hardening of the mounting media. Cells were then imaged using a Nikon Structured Illumination microscope. Images were first processed using the Nikon software using the default settings. Images were then further processed using IMARIS software.

Cell immunoprecipitation and Western blotting

Cells were collected in lysis buffer (150 mM NaCl, 30 mM Tris, pH 7.5, 1 mM EDTA, 1% TritonX-100, 10% glycerol, 0.5 mM dithiothreitol, and 0.1 mM phenylmethylsulfonyl fluoride, plus proteinase/phosphatase inhibitors [EDTA-free, Thermo Scientific] as in Li *et al*., 2012) approximately 24 h after transfection. Antibody was added and samples were incubated on a nutator overnight at 4°C. The next day, Protein A-Sepharose beads (Sigma) were added and samples were incubated on a nutator for 2 h at 4°C. After washing in lysis buffer, immunoprecipitated proteins were removed from the beads with 2× SDS buffer and run on an 8 or 10% SDS–PAGE gel and transferred to a nitrocellulose membrane. Westerns were visualized using x-ray film or the Typhoon Imager. Primary antibodies were: anti-GFP (JL-8; Clontech, 1:1000), anti-Flag (Sigma-Aldrich, 1:2000), and anti-γ-tubulin (Sigma-Aldrich, 1:2000). Secondary antibodies were: IRDye800CW anti-mouse (Licor 1:10,000); HRP–conjugated anti-mouse (Sigma 1:1000).

MS

HEK293T cells were transfected with pCMV-Flag-Drosophila-APC2 and stable cell lines where established using puromycin resistance. Immunoblotting was used to confirm expression. M2 anti-FLAG antibody (Sigma) was used to pull down Flag-APC2. Cells were

washed 3× with PBS and then harvested in RIPA buffer. The lysate was precleared with protein A beads for 2 h at 4°C before the anti-FLAG antibody was added overnight at 4°C. Next day, protein A beads were added to the samples and incubated for 2 h at 4°C. Washes were conducted with RIPA buffer. Trypsin digestion was performed to elute proteins/peptides.

Trypsinized peptides were separated by reverse-phase liquid chromatography using a nanoACQUITY UPLC system (Waters Corporation). Peptides were trapped on a 2 cm column (Pepmap 100, 3 µm particle size, 100 Å pore size) and separated on a 25 cm EASYspray analytical column (75 µm internal diameter, 2.0 µm C18 particle size, 100 Å pore size). The analytical column was heated to 35°C. A 150 min gradient from 1% buffer B (0.1% formic acid in acetonitrile) to 35% buffer B at flowing at 300 nl/min was used. MS analysis was performed by an Orbitrap Elite mass spectrometer (Thermo Scientific). The ion source was operated at 2.6 kV with the ion transfer tube temperature set to 300°C. Full MS scans (300–2000 m/z) were acquired by the Orbitrap analyzer at 120,000 resolution, and data-dependent MS2 spectra were acquired in the linear ion trap on the 15 most intense ions using a 2.0 m/z isolation window and collision-induced dissociation (35% normalized collision energy). Precursor ions were selected based on charge states (+2 and +3) and intensity thresholds (above 1e5) from the full scan; dynamic exclusion was set to one repeat during 30 s and a 60 s exclusion time. A lock mass of 445.120030 was used.

Raw MS data files were searched in MaxQuant (1.6.2.3) using the following parameters: specific tryptic digestion with up to two missed cleavages, carbamidomethyl fixed modification, variable protein N-terminal acetylation and methionine oxidation, match between runs, LFQ with minimum ratio count of 2, and the UniProtKB/Swiss-Prot human canonical and isoform sequence database (release 02/2017). A 1% false discovery rate was applied to all protein identifications. The MS proteomics data have been deposited to the ProteomeXchange Consortium via the PRIDE [1] partner repository with the dataset identifier PXD016314.

FRAP

FRAP assays were conducted as previously described (Pronobis *et al*., 2015). In short, cells expressing the indicated constructs were imaged 24–48 h after transfection using an Eclipse TE2000-E microscope (Nikon, Japan). Movies were taken at 1 frame/3 s or 1 frame/6 s for 20 min and bleaching was conducted for 8 s with 100% laser power. Movies were processed using the FRAP analyzer in ImageJ. The bleached area and the cell were outlined, background was subtracted, and the movie was processed with FRAP profiler. Values were normalized and recovery plateau and standard error were calculated by averaging 10 movies. For $t_{1/2}$ values were processed in GraphPad (La Jolla, CA) using nonlinear regression (curve fit)-one phase decay. The $t_{1/2}$ values of 10 movies were averaged and standard error was calculated.

ACKNOWLEDGMENTS

Thanks to M. Bienz, Y. Ahmed, J. Axelrod, T. Uemura, the Bloomington Drosophila Stock Center, and the DSHB for key reagents; E. Thornton-Kolbe for lab management; T. Perdue for help with confocal and superresolution microscopy; A. Spracklen and other lab members for helpful advice and suggestions on the manuscript; and the reviewers for useful suggestions. This work was supported by National Institutes of Health R35 GM118096 to M.P. K.N.S. was supported by National Science Foundation Graduate Fellowship DGE-1650116. M.I.P. was supported by a Howard Hughes Medical Institute International Student Research Fellowship.

REFERENCES

Axelrod JD (2001). Unipolar membrane association of Dishevelled mediates Frizzled planar cell polarity signaling. Genes Dev 15, 1182–1187.

Banani SF, Lee HO, Hyman AA, Rosen MK (2017). Biomolecular condensates: organizers of cellular biochemistry. Nat Rev Mol Cell Biol 18, 285–298.

Basson MA (2012). Signaling in cell differentiation and morphogenesis. Cold Spring Harb Perspect Biol 4, a008151.

Bernatik O, Ganji RS, Dijksterhuis JP, Konik P, Cervenka I, Polonio T, Krejci P, Schulte G, Bryja V (2011). Sequential activation and inactivation of Dishevelled in the Wnt/beta-catenin pathway by casein kinases. J Biol Chem 286, 10396–10410.

Bernatik O, Sedova K, Schille C, Ganji RS, Cervenka I, Trantirek L, Schambony A, Zdrahal Z, Bryja V (2014). Functional analysis of dishevelled-3 phosphorylation identifies distinct mechanisms driven by casein kinase 1 and frizzled5. J Biol Chem 289, 23520–23533.

Bilic J, Huang YL, Davidson G, Zimmermann T, Cruciat CM, Bienz M, Niehrs C (2007). Wnt induces LRP6 signalosomes and promotes dishevelled-dependent LRP6 phosphorylation. Science 316, 1619–1622.

Brand AH, Perrimon N (1993). Targeted gene expression as a means of altering cell fates and generating dominant phenotypes. Development 118, 401–415.

Cliffe A, Hamada F, Bienz M (2003). A role of Dishevelled in relocating Axin to the plasma membrane during wingless signaling. Curr Biol 13, 960–966.

Dajani R, Fraser E, Roe SM, Yeo M, Good VM, Thompson V, Dale TC, Pearl LH (2003). Structural basis for recruitment of glycogen synthase kinase 3beta to the axin-APC scaffold complex. EMBO J 22, 494–501.

DeBruine ZJ, Xu HE, Melcher K (2017). Assembly and architecture of the Wnt/beta-catenin signalosome at the membrane. Br J Pharmacol 174, 4564–4574.

DiNardo S, Sher E, Heemskerk-Jongens J, Kassis JA, O'Farrell P (1988). Two-tiered regulation of spatially patterned *engrailed* gene expression during *Drosophila* embryogenesis. Nature 332, 604–609.

Duffy JB (2002). GAL4 system in Drosophila: a fly geneticist's Swiss army knife. Genesis 34, 1–15.

Fagotto F, Jho EH, Zeng L, Kurth T, Joos T, Kaufmann C, Costantini F (1999). Domains of Axin involved in protein-protein interactions, Wnt pathway inhibition, and intracellular localization. J Cell Biol 145, 741–756.

Faux MC, Coates JL, Catimel B, Cody S, Clayton AH, Layton MJ, Burgess AW (2008). Recruitment of adenomatous polyposis coli and beta-catenin to axin-puncta. Oncogene 27, 5808–5820.

Fiedler M, Mendoza-Topaz C, Rutherford TJ, Mieszczanek J, Bienz M (2011). Dishevelled interacts with the DIX domain polymerization interface of Axin to interfere with its function in down-regulating beta-catenin. Proc Natl Acad Sci USA 108, 1937–1942.

Gammons M, Bienz M (2017). Multiprotein complexes governing Wnt signal transduction. Curr Opin Cell Biol 51, 42–49.

Gammons MV, Renko M, Johnson CM, Rutherford TJ, Bienz M (2016a). Wnt Signalosome Assembly by DEP Domain Swapping of Dishevelled. Mol Cell 64, 92–104.

Gammons MV, Rutherford TJ, Steinhart Z, Angers S, Bienz M (2016b). Essential role of the Dishevelled DEP domain in a Wnt-dependent human-cell-based complementation assay. J Cell Sci 129, 3892–3902.

Gonzalez-Sancho JM, Brennan KR, Castelo-Soccio LA, Brown AM (2004). Wnt proteins induce dishevelled phosphorylation via an LRP5/6-independent mechanism, irrespective of their ability to stabilize beta-catenin. Mol Cell Biol 24, 4757–4768.

Gonzalez-Sancho JM, Greer YE, Abrahams CL, Takigawa Y, Baljinnyam B, Lee KH, Lee KS, Rubin JS, Brown AM (2013). Functional consequences of Wnt-induced dishevelled 2 phosphorylation in canonical and noncanonical Wnt signaling. J Biol Chem 288, 9428–9437.

Harnoš J, Ryneš J, Víšková P, Foldynová-Trantírková S, Bajard-Ešner L, Trantírek L, Bryja V (2018). Analysis of binding interfaces of the human scaffold protein AXIN1 by peptide microarrays. J Biol Chem 293, 16337–16347.

Hart M, Concordet JP, Lassot I, Albert I, del los Santos R, Durand H, Perret C, Rubinfeld B, Margottin F, Benarous R, Polakis P (1999). The F-box protein beta-TrCP associates with phosphorylated beta-catenin and regulates its activity in the cell. Curr Biol 9, 207–210.

Hilger M, Mann M (2012). Triple SILAC to determine stimulus specific interactions in the Wnt pathway. J Proteome Res 11, 982–994.

Jiang J, Struhl G (1998). Regulation of the Hedgehog and Wingless signaling pathways by the F-Box/WD-40-repeat protein Slimb. Nature 391, 493–496.

Julius MA, Schelbert B, Hsu W, Fitzpatrick E, Jho E, Fagotto F, Costantini F, Kitajewski J (2000). Domains of axin and disheveled required for interaction and function in wnt signaling. Biochem Biophys Res Commun 276, 1162–1169.

Kan W, Enos M, Korkmazhan E, Muennich S, Chen D-H, Gammons MV, Vasishtha M, Bienz M, Dunn AR, Skiniotis G, Weis WI (2020). Limited Dishevelled/Axin oligomerization determines efficiency of Wnt/β-catenin signal transduction. bioRxiv doi: 10.1101/2020.04.01.020057.

Kishida M, Hino S, Michiue T, Yamamoto H, Kishida S, Fukui A, Asashima M, Kikuchi A (2001). Synergistic activation of the Wnt signaling pathway by Dvl and casein kinase Iepsilon. J Biol Chem 276, 33147–33155.

Kishida S, Yamamoto H, Hino SI, Ikeda S, Kishida M, Kikuchi A (1999). DIX domains of Dvl and axin are necessary for protein interactions and their ability to regulate beta-catenin stability. Mol Cell Biol 19, 4414–4422.

Kitagawa M, Hatakeyama S, Shirane M, Matsumoto M, Ishida N, Hattori K, Nakamichi I, Kikuchi A, Nakayama KI, Nakayama K (1999). An F-box protein, FWD1, mediates ubiquitin-dependent proteolysis of beta-catenin. EMBO J 18, 2401–2410.

Klingensmith J, Nusse R, Perrimon N (1994). The *Drosophila* segment polarity gene *dishevelled* encodes a novel protein required for response to *wingless* signal. Genes Dev 8, 118–130.

Kunttas-Tatli E, Roberts DM, McCartney BM (2014). Self-association of the APC tumor suppressor is required for the assembly, stability, and activity of the Wnt signaling destruction complex. Mol Biol Cell 25, 3424–3436.

Lee EK, Diehl JA (2014). SCFs in the new millennium. Oncogene 33, 2011–2018.

Li VS, Ng SS, Boersema PJ, Low TY, Karthaus WR, Gerlach JP, Mohammed S, Heck AJ, Maurice MM, Mahmoudi T, Clevers H (2012). Wnt signaling through inhibition of beta-catenin degradation in an intact Axin1 complex. Cell 149, 1245–1256.

Liu C, Kato Y, Zhang Z, Do VM, Yankner BA, He X (1999). beta-Trcp couples beta-catenin phosphorylation-degradation and regulates Xenopus axis formation. Proc Nat Acad Sci USA 96, 6273–6278.

Liu C, Li Y, Semenov M, Han C, Baeg GH, Tan Y, Zhang Z, Lin X, He X (2002). Control of beta-catenin phosphorylation/degradation by a dual-kinase mechanism. Cell 108, 837–847.

Liu J, Stevens J, Matsunami N, White RL (2004). Targeted degradation of beta-catenin by chimeric F-box fusion proteins. Biochem Biophys Res Commun 313, 1023–1029.

MacDonald BT, He X (2012). Frizzled and LRP5/6 receptors for Wnt/beta-catenin signaling. Cold Spring Harb Perspect Biol 4, a007880.

Major MB, Camp ND, Berndt JD, Yi X, Goldenberg SJ, Hubbert C, Biechele TL, Gingras AC, Zheng N, Maccoss MJ, *et al*. (2007). Wilms tumor suppressor WTX negatively regulates WNT/beta-catenin signaling. Science 316, 1043–1046.

Marikawa Y, Elinson RP (1998). beta-TrCP is a negative regulator of Wnt/beta-catenin signaling pathway and dorsal axis formation in Xenopus embryos. Mech Dev 77, 75–80.

McCartney BM, Dierick HA, Kirkpatrick C, Moline MM, Baas A, Peifer M, Bejsovec A (1999). Drosophila APC2 is a cytoskeletally-associated protein that regulates Wingless signaling in the embryonic epidermis. J Cell Biol 146, 1303–1318.

Mendoza-Topaz C, Mieszczanek J, Bienz M (2011). The APC tumour suppressor is essential for Axin complex assembly and function, and opposes Axin's interaction with Dishevelled. Biol Open 1, 110013.

Metcalfe C, Mendoza-Topaz C, Mieszczanek J, Bienz M (2010). Stability elements in the LRP6 cytoplasmic tail confer efficient signalling upon DIX-dependent polymerization. J Cell Sci 123, 1588–1599.

Miller JR, Rowning BA, Larabell CA, Yang-Snyder JA, Bates RL, Moon RT (1999). Establishment of the dorsal/ventral axis in Xenopus embryos coincides with the dorsal enrichment of dishevelled that is dependent on cortical rotation. J Cell Biol 146, 427–438.

Noordermeer J, Klingensmith J, Perrimon N, Nusse R (1994). *dishevelled* and *armadillo* act in the *wingless* signaling pathway. Nature 367, 80–83.

Nusse R, Clevers H (2017). Wnt/beta-catenin signaling, disease, and emerging therapeutic modalities. Cell 169, 985–999.

Orford K, Crockett C, Jensen JP, Weissman AM, Byers SW (1997). Serine phosphorylation-regulated ubiquitination and degradation of beta-catenin. J Biol Chem 272, 24735–24738.

Pedersen NM, Thorvaldsen TE, Schultz SW, Wenzel EM, Stenmark H (2016). Formation of tankyrase inhibitor-induced degradasomes requires proteasome activity. PLoS One 11, e0160507.

Peifer M, Sweeton D, Casey M, Wieschaus E (1994). *wingless* signal and Zeste-white 3 kinase trigger opposing changes in the intracellular distribution of Armadillo. Development 120, 369–380.

Peters JM, McKay RM, McKay JP, Graff JM (1999). Casein kinase I transduces Wnt signals. Nature 401, 345–350.

Polakis P (1997). The adenomatous polyposis coli (APC) tumor suppressor. Biochimica et Biophysica Acta 1332, F127–F147.

Price MH, Roberts DM, McCartney BM, Jezuit E, Peifer M (2006). Cytoskeletal dynamics and cell signaling during planar polarity establishment in the Drosophila embryonic denticle. J Cell Sci 119, 403–415.

Pronobis MI, Deuitch N, Posham V, Mimori-Kiyosue Y, Peifer M (2017). Reconstituting regulation of the canonical Wnt pathway by engineering a minimal beta-catenin destruction machine. Mol Biol Cell 28, 41–53.

Pronobis MI, Rusan NM, Peifer M (2015). A novel GSK3-regulated APC:Axin interaction regulates Wnt signaling by driving a catalytic cycle of efficient betacatenin destruction. eLife 4, e08022.

Roberts DM, Pronobis MI, Poulton JS, Kane EG, Peifer M (2012). Regulation of Wnt signaling by the tumor suppressor APC does not require ability to enter the nucleus nor a particular cytoplasmic localization. Mol Biol Cell 23, 2041–2056.

Roberts DM, Pronobis MI, Poulton JS, Waldmann JD, Stephenson EM, Hanna S, Peifer M (2011). Deconstructing the beta-catenin destruction complex: mechanistic roles for the tumor suppressor APC in regulating Wnt signaling. Mol Biol Cell 22, 1845–1863.

Robertson H, Hayes JD, Sutherland C (2018). A partnership with the proteasome; the destructive nature of GSK3. Biochem Pharmacol 147, 77–92.

Sakanaka C, Leong P, Xu L, Harrison SD, Williams LT (1999). Casein kinase I-epsilon in the Wnt pathway: Regulation of beta-catenin function. Proc Nat Acad Sci USA 96, 12548–12552.

Schaefer KN, Bonello TT, Zhang S, Williams CE, Roberts DM, McKay DJ, Peifer M (2018). Supramolecular assembly of the beta-catenin destruction complex and the effect of Wnt signaling on its localization, molecular size, and activity in vivo. PLoS Genet 14, e1007339.

Schaefer KN, Peifer M (2019). Wnt/Beta-catenin signaling regulation and a role for biomolecular condensates. Dev Cell 48, 429–444.

Schwarz-Romond T, Fiedler M, Shibata N, Butler PJ, Kikuchi A, Higuchi Y, Bienz M (2007a). The DIX domain of Dishevelled confers Wnt signaling by dynamic polymerization. Nat Struct Mol Biol 14, 484–492.

Schwarz-Romond T, Merrifield C, Nichols BJ, Bienz M (2005). The Wnt signalling effector Dishevelled forms dynamic protein assemblies rather than stable associations with cytoplasmic vesicles. J Cell Sci 118, 5269–5277.

Schwarz-Romond T, Metcalfe C, Bienz M (2007b). Dynamic recruitment of axin by Dishevelled protein assemblies. J Cell Sci 120, 2402–2412.

Shimada Y, Usui T, Yanagawa S, Takeichi M, Uemura T (2001). Asymmetric colocalization of Flamingo, a seven-pass transmembrane cadherin, and Dishevelled in planar cell polarization. Curr Biol 11, 859–863.

Spink KE, Polakis P, Weis WI (2000). Structural basis of the Axin-adenomatous polyposis coli interaction. EMBO J 19, 2270–2279.

Stamos JL, Weis WI (2013). The beta-catenin destruction complex. Cold Spring Harb Perspect Biol 5, a007898.

Stamos JL, Chu ML, Enos MD, Shah N, Weis WI (2014). Structural basis of GSK-3 inhibition by N-terminal phosphorylation and by the Wnt receptor LRP6. eLife 3, e01998.

Su Y, Fu C, Ishikawa S, Stella A, Kojima M, Shitoh K, Schreiber EM, Day BW, Liu B (2008). APC is essential for targeting phosphorylated beta-catenin to the SCFbeta-TrCP ubiquitin ligase. Mol Cell 32, 652–661.

Tamai K, Zeng X, Liu C, Zhang X, Harada Y, Chang Z, He X (2004). A mechanism for Wnt coreceptor activation. Mol Cell 13, 149–156.

Tauriello DV, Jordens I, Kirchner K, Slootstra JW, Kruitwagen T, Bouwman BA, Noutsou M, Rudiger SG, Schwamborn K, Schambony A, Maurice MM (2012). Wnt/beta-catenin signaling requires interaction of the Dishevelled DEP domain and C terminus with a discontinuous motif in Frizzled. Proc Natl Acad Sci USA 109, E812–E820.

Thorvaldsen TE, Pedersen NM, Wenzel EM, Schultz SW, Brech A, Liestol K, Waaler J, Krauss S, Stenmark H (2015). Structure, dynamics, and functionality of tankyrase inhibitor-induced degradasomes. Mol Cancer Res 13, 1487–1501.

van Leeuwen F, Samos CH, Nusse R (1994). Biological activity of soluble wingless protein in cultured Drosophila imaginal disc cells. Nature 368, 342–344.

Wang Z, Tacchelly-Benites O, Yang E, Thorne CA, Nojima H, Lee E, Ahmed Y (2016). Wnt/Wingless pathway activation is promoted by a critical threshold of axin maintained by the tumor suppressor APC and the ADP-ribose polymerase tankyrase. Genetics 203, 269–281.

Wehrli M, Dougan ST, Caldwell K, O'Keefe L, Schwartz S, Vaizel-Ohayon D, Schejter E, Tomlinson A, DiNardo S (2000). *arrow* encodes an LDL-receptor-related protein essential for Wingless signalling. Nature 407, 527–530.

Wieschaus E, Nüsslein-Volhard C (1986). Looking at embryos. In: Drosophila, A Practical Approach, ed. DB Roberts, Oxford, England: IRL Press, 199–228.

Willert K, Logan CY, Arora A, Fish M, Nusse R (1999). A Drosophila Axin homolog, Daxin, inhibits Wnt signaling. Development 126, 4165–4173.

Wojcik EJ, Glover DM, Hays TS (2000). The SCF ubiquitin ligase protein slimb regulates centrosome duplication in Drosophila. Curr Biol 10, 1131–1134.

Wu G, Xu G, Schulman BA, Jeffrey PD, Harper JW, Pavletich NP (2003). Structure of a beta-TrCP1-Skp1-beta-catenin complex: destruction motif binding and lysine specificity of the SCF(beta-TrCP1) ubiquitin ligase. Mol Cell 11, 1445–1456.

Xu W, Kimelman D (2007). Mechanistic insights from structural studies of beta-catenin and its binding partners. J Cell Sci 120, 3337–3344.

Yamanishi K, Fiedler M, Terawaki SI, Higuchi Y, Bienz M, Shibata N (2019). A direct heterotypic interaction between the DIX domains of Dishevelled and Axin mediates signaling to beta-catenin. Sci Signal 12, eaaw5505.

Yanagawa S, van Leeuwen F, Wodarz A, Klingensmith J, Nusse R (1995). The dishevelled protein is modified by wingless signaling in Drosophila. Genes Dev 9, 1087–1097.

Yang-Snyder J, Miller JR, Brown JD, Lai C-J, Moon RT (1996). A *frizzled* homolog functions in a vertebrate *Wnt* signaling pathway. Curr Biol 6, 1302–1306.